UNIVERSITY OF CALIFORNIA SAN DIEGO

Anatomy and function of higher-order thalamocortical circuits in the visual system

A Dissertation submitted in partial satisfaction of the requirements for the degree

Doctor of Philosophy

in

Neurosciences

by

Rachel M. Cassidy

Committee in charge:

Professor Edward Callaway, Chair
Professor Christina Gremel, Co-Chair
Professor Byungkook Lim
Professor Eran Mukamel
Professor John Reynolds

2023

The Dissertation of Rachel Cassidy is approved, and it is acceptable in quality and form for publication on microfilm and electronically.

University of California San Diego

2023

TABLE OF CONTENTS

LIST OF FIGURES

.

LIST OF TABLES

LIST OF ABBREVIATIONS

A	anterior area
AM	anteromedial area
AL	anterolateral area
AUD	auditory cortex
CT	corticothalamic
dLGN	dorsal lateral geniculate nucleus
FO	first-order (thalamic nucleus)
HO	higher-order (thalamic nucleus)
HVA	higher visual area
ISI	intrinsic signal imaging
L5, L6, etc.	cortical layer 5, 6, etc.
LI	laterointermediate area
LM	lateromedial area
P	posterolateral area
PM	posteromedial area
POR	postrhinal area
PPC	posterior parietal cortex
PTN	pretectal nuclei
RL	rostrolateral area
RSP	retrosplenial cortex
RVdG	glycoprotein-deleted rabies virus
SC	superior colliculus

SS	somatosensory cortex
TC	thalamocortical
TRN	thalamic reticular nucleus
V1	primary visual cortex

ACKNOWLEDGEMENTS

I would like to thank my advisor, Professor Ed Callaway, for his mentorship and for always treating me as a competent and independent scientist. I thank Dr. Euiseok Kim for thoughtful discussions and technical guidance at the crucial early stages of this dissertation work. I thank Dr. Megan Kirchgessner for her technical support and helpful scientific discussions. I acknowledge the technical assistance of Angel Macias, Will Nuñez-Lagos, and Genevieve Ugorji, without which this work would not have been possible. I would also like to thank all the members of the Callaway lab for cultivating an intellectually stimulating and emotionally supportive environment. I thank my thesis committee for their thoughtful advice and encouragement.

Thank you to my friends and family who have supported me throughout my graduate training. In particular, I am eternally grateful to Ryan Sema for his patience, encouragement, and unconditional support.

Chapter 1, in full, is currently being prepared for submission for publication and will include Angel Macias, Will N. Lagos, and Genevieve Ugorji as co-authors and Professor Edward Callaway as the senior author. The dissertation author was the primary researcher and author of this material.

Chapter 2 contains unpublished material coauthored with Professor Edward Callaway. The dissertation author was the primary author of this chapter.

VITA

2013 Bachelor of Science in Biomedical Engineering, Northwestern University

2023 Doctor of Philosophy in Neurosciences, Computational Neuroscience Specialization
University of California San Diego

ABSTRACT OF THE DISSERTATION

Anatomy and function of higher-order thalamocortical circuits in the visual system

by

Rachel Cassidy

Doctor of Philosophy in Neurosciences

University of California San Diego, 2023

Professor Edward Callaway, Chair
Professor Christina Gremel, Co-Chair

One of the fundamental jobs of the brain is to transform stimuli from the external environment into flexible behavioral outputs. In mammals, thalamocortical circuits perform many of the functions that underlie this complex sensory processing. First-order (FO) thalamic nuclei, such as the dorsal lateral geniculate nucleus (dLGN), relay incoming signals to the cortex, which generates a percept and motor commands. This initial path from the FO thalamus to the cortex is well understood, but interactions between the cortex and higher-order (HO) nuclei, like the pulvinar, remain a mystery. Competing theories on the role of cortico-pulvino-cortical circuits remain unresolved. One model suggests that HO nuclei serve as relays for information transmission between cortical areas; while the alternative proposes a modulatory function

promoted by reciprocal thalamocortical loops. Advances in viral tools for anatomical tracing and targeted perturbation of neuronal activity now allow us to test these hypotheses. This dissertation investigates the anatomical and functional relationship between the pulvinar and extrastriate cortex in the mouse in an attempt to understand the nature of higher-order thalamocortical interactions. In Chapter 1, we map the input/output relationships of distinct projection classes in the pulvinar. Using monosynaptic g-deleted rabies virus, we show that driving layer 5 cortical inputs to the pulvinar are organized as a feedforward, transthalamic relay. We also describe a broad network of modulatory layer 6 inputs which are biased towards reciprocal connections with the pulvinar. Bottom-up input from the superior colliculus (SC) targets every cortical pathway through the pulvinar. Chapter 2 investigates the functional contribution of a pulvinar → extrastriate pathway to visual activity *in vivo* in awake, passively viewing animals. We selectively target a single pulvinar projection population for optogenetic inactivation and compare the effects to inactivation of the FO pathway. Unlike FO thalamocortical input, which is necessary for sensory transmission, the HO input to cortex is not responsible for sensory responses. Instead, our results support a modulatory, excitatory contribution of the pulvinar to cortical activity. In summary, this study establishes a general framework for the anatomical organization of HO thalamocortical circuits, whereby the pulvinar provides a parallel path between cortical areas and a secondary route for bottom-up visual signals. Our physiological results highlight the folly in inferring circuit function from anatomy alone, however, as this transthalamic pathway does not drive visual activity under passive, head-fixed conditions. Instead, our findings describe a *potential* driving pathway between sensory cortices which might relay a non-sensory or context-dependent message. Additional functional studies that engage this circuit in active behavioral states will be necessary to solve the puzzle of the pulvinar.

CHAPTER 1: Complementary input/output organization of cortico-thalamo-cortical pathways

ABSTRACT

Corticocortical projections in the visual system facilitate the hierarchical processing of sensory information. In addition to these direct connections, visual cortical areas are extensively and reciprocally connected to the pulvinar nucleus of the thalamus. Whether these cortico-thalamo-cortical pathways provide a parallel channel for sensory transmission between cortical areas or whether they make reciprocal connections depends on the input/output relationships of the pulvinar. We systematically mapped the brain-wide inputs to different projection populations in the pulvinar. Using G-deleted rabies in adult male and female mice, we traced inputs to populations of pulvinar neurons projecting to each of five higher visual areas (HVAs). HVAs were uniquely mapped using intrinsic signal imaging, and post-mortem sections were aligned to these functional maps. This comprehensive study revealed circuit motifs that were common across target cortical areas. Consistent with a feedforward relay, "driving" cortical inputs from L5 predominantly originate from V1, regardless of the target HVA. L5 inputs were also located in other HVAs, but they were notably absent from the target HVA, consistent with the "no strong loops" hypothesis. Unlike L5 inputs, "modulating" L6 inputs were distributed and overrepresented in the target HVA. These findings establish complementary connection rules for the two cortical pathways to the pulvinar, where L5 inputs avoid reciprocal connections and support feedforward trans-thalamic relays, and L6 inputs are biased toward reciprocal connections, reminiscent of the feedback from V1 L6 to the dLGN.

INTRODUCTION

> *The visual cortex might contain an essentially perfect anatomical hierarchy that has been imperfectly studied using inherently 'noisy' methods of anatomical analysis…To distinguish incisively among different alternatives, however, it is crucial that reports of anatomical connectivity be as precise and quantitative as possible with regard to basic questions of (1) the confidence with which sources and targets have been identified in relation to areal boundaries and (2) the exact laminar distribution of anterograde and retrograde tracers.*
>
> *-Felleman and Van Essen, 1991*

An animal's perception and interactions with the external world rely on incoming sensory information. In the mammalian visual system, the dorsal lateral geniculate nucleus (dLGN) of the thalamus relays this information to the neocortex, where a network of hierarchically organized areas processes increasingly complex features. This hierarchical pathway has been classically defined by the properties of direct corticocortical projections[1,2]. However, thalamic input to this network is not limited to the dLGN pathway; in fact, every level of the visual cortex receives additional input from a higher-order thalamic nucleus, the pulvinar. Unlike the dLGN, the pulvinar is an associative nucleus that receives most of its input from the cortex. This bidirectional connectivity with the visual cortex could allow the pulvinar to route sensory information between cortical areas independently from the direct pathway[3]. The pulvinar also relays subcortical signals from the superior colliculus (SC) and the retina[4–7]. These additional higher-order thalamic pathways could add complexity to the canonical hierarchical model, but

without a comprehensive map of synaptic connections in the pulvinar, its anatomical relationship to the visual network remains unclear.

The mouse is now an established model for studying the visual system, and the availability of viral and genetic tools makes it an ideal system for fine-scale dissection of the input/output connections of the pulvinar (also referred to as the lateral posterior nucleus of the thalamus). As in primates and carnivores, the mouse visual cortex is comprised of the primary visual cortex (V1) and multiple higher visual areas (HVAs) which have hierarchically organized feedforward and feedback connections[2,8–10]. Some evidence suggests that thalamocortical cell types are also similar between species. Relay cells in the primate thalamus are classified as "core" or "matrix" by their differential expression of calcium binding proteins, along with other morphological and synaptic properties[11]. While similar molecular markers have not been found in rodents[12], studies of axonal morphology and synaptic properties have revealed two types of neurons which resemble the primate core and matrix projections[11,13,14]. Diffuse pulvinar projections to V1 target layers 1 and 5a, and they show synaptic properties typical of weak feedback connections[15]. These "matrix" projections also target other cortical areas, including HVAs. "Core" cells in the pulvinar avoid V1 altogether and instead target the middle layers of HVAs, with focal axonal arborizations and stronger synaptic properties. Individual core cells in the rodent pulvinar typically project to only 2-3 brain areas[13]. While pulvinar outputs are therefore not completely independent, they do not broadcast indiscriminately to all visual areas[16,17]. Therefore, projections could send distinct signals to different cortical areas depending on the organization of their inputs.

Cortical input to the pulvinar originates primarily from visual areas, with additional input from non-visual areas such as somatosensory, auditory, motor, and prefrontal cortices[18–21].

Corticothalamic (CT) axons are organized topographically within the pulvinar, with spatial distributions that overlap the cell populations projecting back to those respective cortical regions[16,22,23]. While the coarse input/output organization of the pulvinar is reciprocal, there are some regions of overlap between cortical fields that could support the transthalamic relay of information between areas[3,24]. For a transthalamic pathway to be relevant for information transmission, however, the CT inputs must be capable of driving activity in the pulvinar. Layer 5 CT "drivers" are necessary for visual responses and receptive field structure in the pulvinar, whereas feedback from layer 6 CT "modulators" can affect the frequency and gain of pulvinar responses, but are not required for visual responses[25]. Therefore, understanding both the cortical regions and cell types that connect to pulvinar projections is necessary to describe fine-scale cortico-thalamo-cortical circuits.

One advantage of a parallel pathway through the thalamus is that additional bottom-up signals can be integrated with cortical activity. The pulvinar receives extrageniculate retinal input via the SC, which is necessary for some visual activity in the cortex[4]. The SC shapes velocity tuning in HVAs across the cortical network[22], but it is unclear whether this influence is from direct tecto-pulvinar input to all areas or from more specific projections whose effects are then propagated indirectly. Anterograde tracing of SC projections labels pulvinar regions that project primarily to lateral HVAs[6,23], but due to overlapping cortical projections and extensive dendritic fields, these methods are too coarse to determine whether the tecto-pulvinar pathway targets lateral HVAs selectively.

Determining the fine-scale relationships between the inputs and outputs of the pulvinar requires projection-specific transsynaptic tracing. Recent studies have applied this technique to a limited subset of pulvino-cortical projections[14,17,26], but it is unclear whether those findings can

be generalized across the cortical network. To reveal the general principles that describe pulvino-cortical connections throughout the visual hierarchy, we targeted five different Pulvinar→HVA projection populations (LM, AL, RL, AM, PM) with intrinsic signal imaging and cre-dependent, monosynaptic rabies tracing[27]. The resulting input/output map is the most comprehensive to date. Our data show that V1 is the largest source of driving layer 5 inputs to all HVA-projecting pulvinar populations, confirming the long-standing theory that cortico-thalamo-cortical connections serve as a parallel feedforward relay[3,17]. We also find that L5 specifically avoids reciprocal connections, consistent with the "no strong loops" hypothesis[28]. In contrast, L6 frequently makes reciprocal connections in addition to generalized, nonspecific input from lateral HVAs. Together, the driving and modulating inputs to the pulvinar form complementary pathways. Regardless of the cortical target, all pulvinar populations receive input from the SC. These results show that the pulvinar is organized as a feedforward pathway between cortical areas that reflects the directionality of the existing cortical hierarchy, and that each of these pathways could integrate sensorimotor signals from the SC.

RESULTS

Brain-wide mapping of pulvinar input/output connections

We characterized the brain-wide inputs to specific pulvinar projection neurons by targeting individual higher visual areas for retrograde, cre-dependent monosynaptic rabies tracing. AAV-Cre injections were targeted to functionally mapped cortical areas in wild-type mice (n = 24) to drive cre-dependent expression of the avian TVA receptor (AAV-Flex-TCB) and rabies glycoprotein (AAV-DIO-oG) in pulvinar projection populations (Fig 1.1b). The boundaries of five targeted cortical areas (PM, AM, RL, AL, and LM) vary between individual animals, so we used intrinsic signal imaging to generate retinotopically defined area borders.

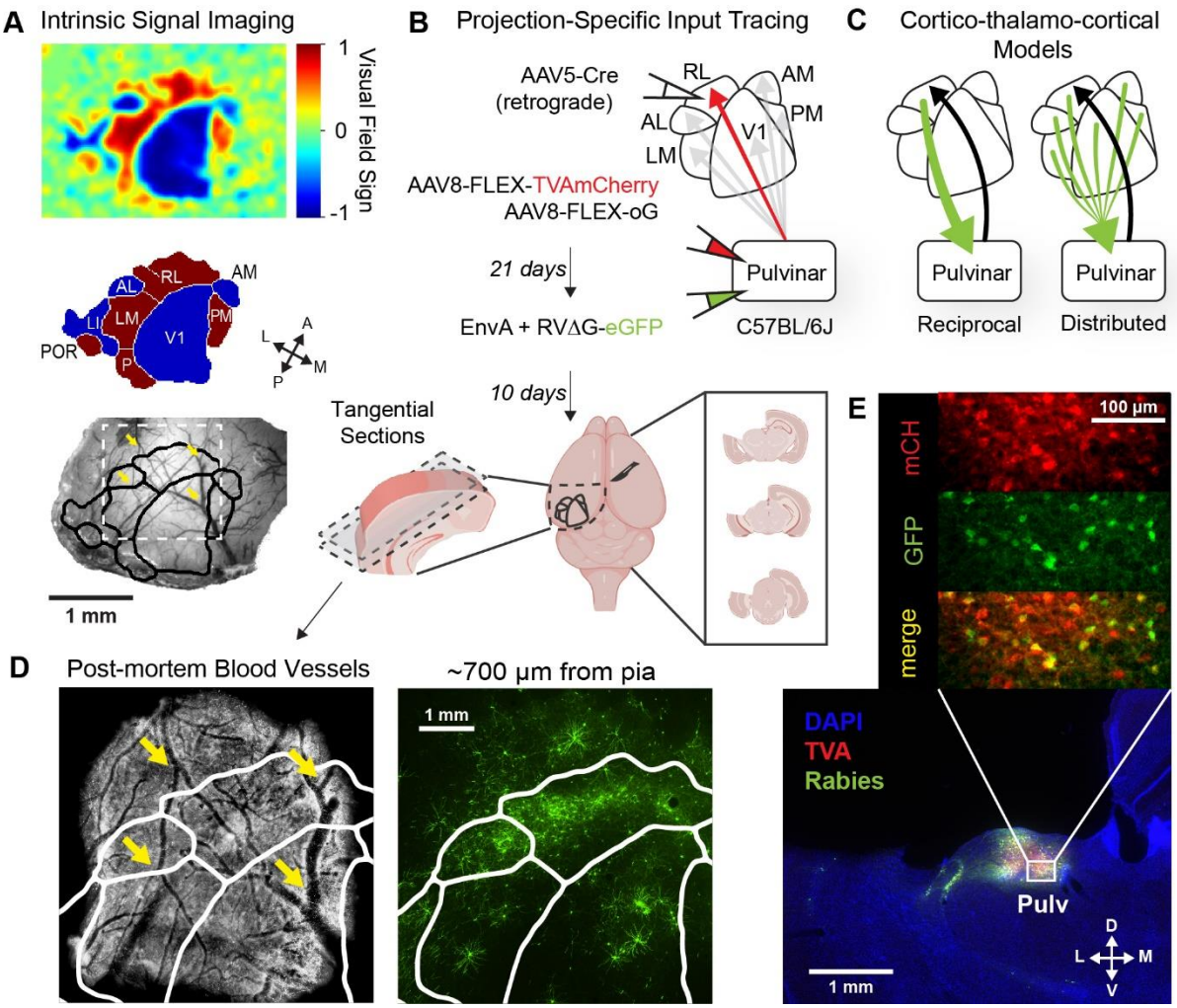

Figure 1.1 Targeting visual areas for pulvino-cortical input tracing. A) Intrinsic signal imaging and automatic segmentation defines HVA borders aligned to *in vivo* blood vessels. **B)** Schematic of viral injection strategy for projection-specific input tracing. (top) AAV-Cre injected into individual HVAs in wild-type mice retrogradely infects pulvinar projection neurons expressing cre-dependent helper viruses. Pseudotyped, g-deleted rabies is injected into the pulvinar to label presynaptic inputs to specific projection populations. (bottom) Visual cortex is dissected and sectioned tangentially to align tissue with the *in vivo* blood vessels and HVA map. The remainder of the tissue is processed to quantify brain-wide inputs. **C)** Models of cortico-thalamo-cortical connectivity. **D)** Tangential cortical sections aligned to the HVA map. (left) Surface blood vessel landmarks in post-mortem tissue are aligned with the in vivo imaging. (right) GFP+ cortico-pulvinar inputs in aligned deeper sections. **E)** Putative starter cells in the pulvinar expressing TVAmCherry and RVΔG-eGFP.

These functional maps guided precise, restricted injections, and they also permitted accurate alignment of post-mortem, tangentially sectioned cortical tissue to the visual areas for quantification of RVdG+ inputs (Fig 1.1B,D). Non-cortical brain areas were sectioned and processed for quantification of brain-wide inputs (Fig 1.1e).

Consistent with previous bulk retrograde tracing, we found that the largest source of input to the pulvinar was the cortex (41.4%), followed by inhibitory inputs from the thalamic reticular nucleus (15.4%) and pretectal nuclei (11.3%; Fig 1.2)). Input from major brain areas did not depend on the cortical target of the traced pulvinar neurons ($p>0.05$, Kruskal-Wallis nonparametric test with Dunn-Šidák post-hoc correction), with the exception of the SC and the zona incerta (ZI). Most target areas followed a similar distribution of these subcortical inputs, but LM-projecting pulvinar neurons received a significantly higher proportion of input from the SC than RL- and AL- projecting pulvinar did (median input - LM: 22.3%; RL: 6.4%, $p_{adj} = 0.0173$; AM: 6.4%, $p_{adj} = 0.0272$, Kruskal-Wallis test with Dunn-Šidák post hoc correction). LM and PM inputs from the zona incerta were slightly, but significantly, different (LM: 3.2%, PM: 6.7%, $p_{adj} = 0.0413$, Kruskal-Wallis test with Dunn-Šidák post hoc correction).

The superior colliculus provides input to all projection populations

To understand which cortical projections might be integrating visual information from the SC, we compared the SC inputs to all HVAs and quantified their laminar and mediolateral position (Fig 1.3). Tectal inputs have been reported to target caudal regions of the pulvinar, where projections to lateral extrastriate areas are concentrated[4,6,15]. The volume and coordinates of our thalamic injections were optimized to cover as much of the cortico-recipient pulvinar as possible, so we expect that the reported SC inputs, particularly in the superficial layers, are undersampled for LM-projecting cases. Even so, we find that all HVAs receive input from the

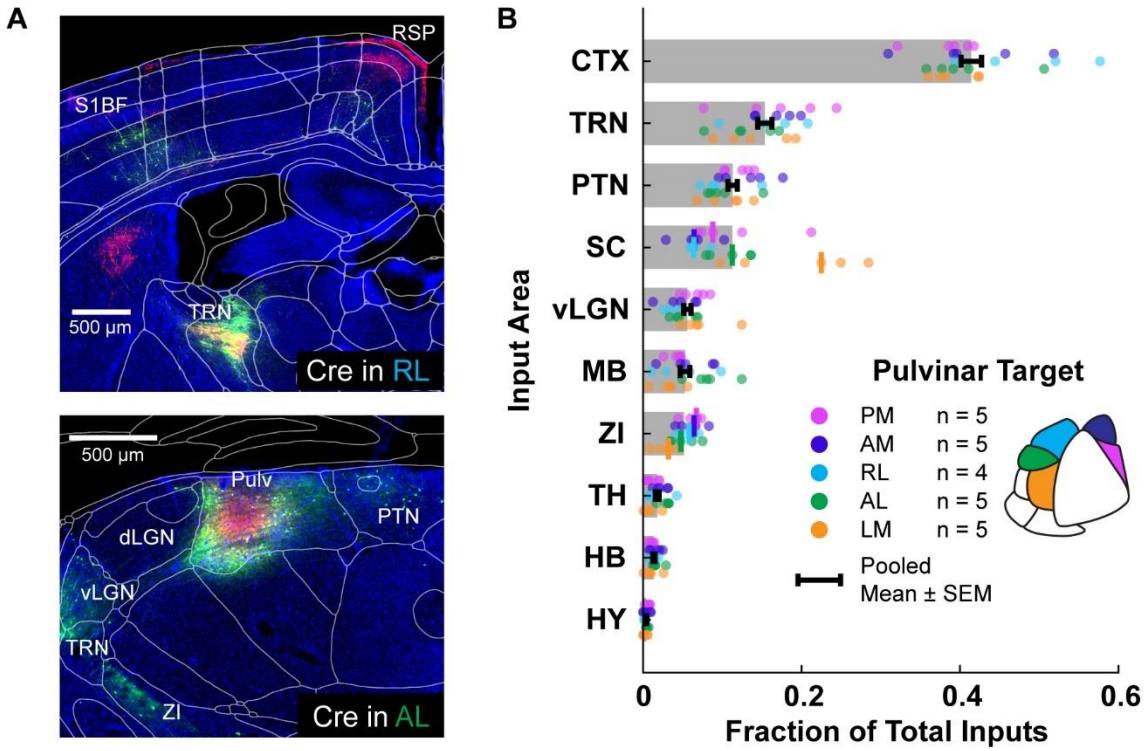

Figure 1.2 Brain-wide inputs to the pulvinar are similar for different projection targets. A) Example coronal sections of cre-dependent rabies labeling in two example experiments with transformed CCF atlas borders. Scale bars = 500 µm.*Top*: RVdG-eGFP+ inputs (green) are labeled in deep layers of somatosensory cortex and the visual subdivision of TRN in an RL-projecting experiment. TVAmCherry+ pulvinar axons (red) are labeled in the upper layers of RSP, the striatum, and the visual TRN. *Bottom*: Starter cells projecting to AL are labeled in the pulvinar (Pulv) with TVAmCherry (red) and RVdG-eGFP (green) but are not found in dLGN. Subcortical RVdG-eGFP+ (green) inputs are labeled in the ZI, vLGN, and PTN. **B)** Inputs to the pulvinar from major divisions of the brain, expressed as a fraction of the total inputs for each animal. Individual animals are plotted with colored markers. Bar lengths represent the mean of the sample obtained by pooling projection targets together. For all areas except for SC and ZI, the distribution of inputs for different projection targets was not significantly different ($p>0.05$, kruskal-wallis test with Dunn-Šidák post-hoc correction for multiple comparisons), and samples were combined for a pooled mean ± SEM represented by black error bars. For areas SC and ZI, the median input for each projection target is displayed by a vertical line. CTX: Cortex; TRN: thalamic reticular nucleus; PTN: pretectal nuclei; SC: superior colliculus; vLGN: ventral subdivision of the lateral geniculate nucleus; MB: midbrain (other); ZI: zona incerta; TH: thalamus (other); HB: hindbrain; HY: hypothalamus (other); S1BF: primary somatosensory barrel field; RSP: retrosplenial cortex; dLGN: dorsal subdivision of the lateral geniculate nucleus

tecto-pulvinar pathway, which is a marked anatomical difference from the primate visual system, in which only dorsal stream areas receive tectal input[7]. These SC inputs to anterior and medial HVAs were concentrated in deeper layers of the SC, and therefore may serve to relay premotor, rather than sensory, information. LM was the only HVA targeted where some injections did not cover the full spatial extent of the projection population. All injections covered the cortico-recipient portion of this region, but only 3/5 also sufficiently covered the caudolateral pulvinar where the widefield vertical cells of the SCsg project to. This bimodality is evident in the breakdown of inputs by layer for LM (Fig 1.3b), and we believe that the true proportion of superficial SC inputs to LM-projecting cells is likely closer to the larger of the two modes.

Like the pulvinar and cortex, the SC is retinotopically organized, with variation across the mediolateral SC axis corresponding to the elevation gradient. Recent work has demonstrated that corticotectal projections are systematically distributed along a polar SC axis[29], so we wanted to know if the SC-pulvinar inputs shared that organization. By quantifying the positions of SC input neurons to each thalamocortical projection group, we discovered an ordered trend of cell positions reminiscent of the corticotectal organization (Fig 1.3 D-E). Inputs to LM-projecting and PM-projecting neurons were concentrated in the most medial portions of the SC, corresponding to upper visual fields. Inputs to RL-, AL-, and AM- projecting neurons were more laterally distributed. Inputs to RL- and AM- projections even extended slightly into regions of the SC which are multimodal and could receive somatosensory and/or auditory inputs.

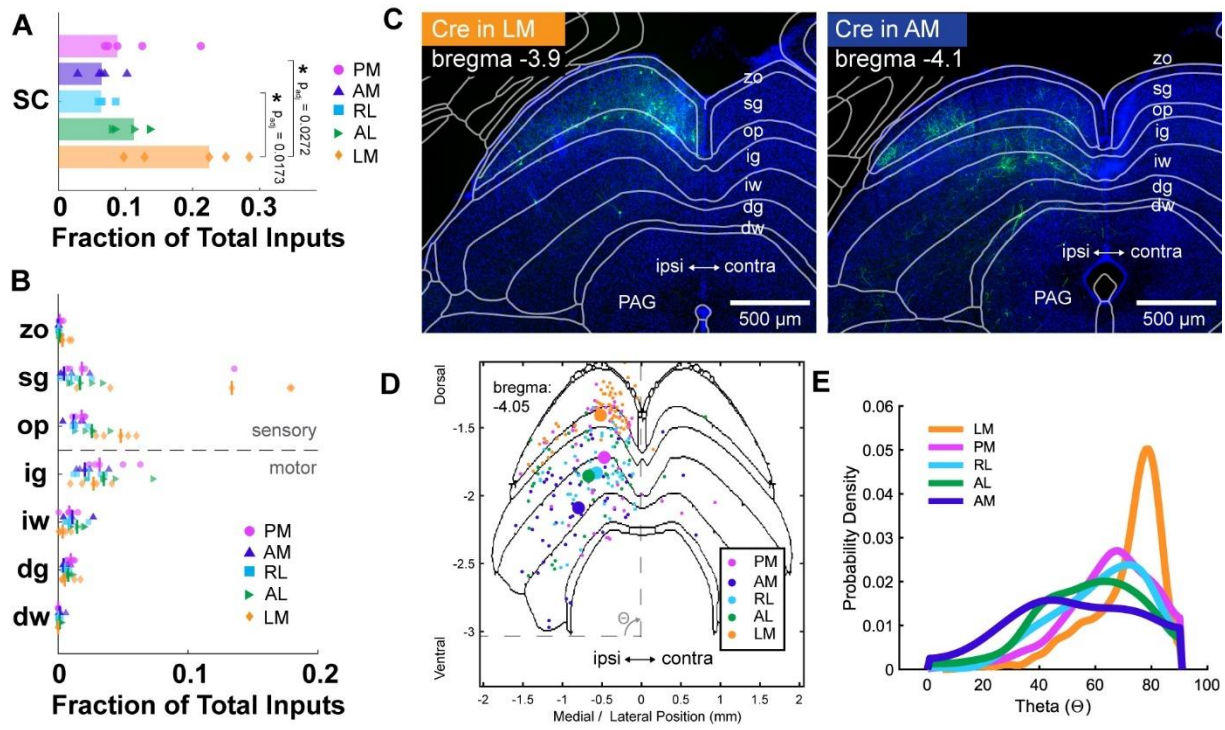

Figure 1.3 Superior Colliculus targets all pulvino-cortical projection populations. A) SC input to PM- (magenta), AM- (purple), RL- (cyan), AL- (green), and LM-projecting (orange) pulvinar neurons. Bar lengths correspond to the median SC input expressed as a fraction of total inputs. Input to LM-projecting neurons was significantly greater than to AM- (p_{adj}=0.0272) and RL- (p_{adj}=0.0173) projecting neurons as determined by a Kruskal-Wallis nonparametric rank test with Dunn-Šidák post-hoc correction for multiple comparisons. All other pairwise comparisons were nonsignificant. **B)** SC input from each layer. All projection populations receive input from both sensory and motor layers of SC. zo: zonal; sg: superficial gray; op: optic; ig: intermediate gray; iw: intermediate white; dg: deep gray; dw: deep white. **C)** Example coronal sections of SC inputs (green) in an LM-projecting (left) and AM-projecting (right) animal with transformed CCF borders. Scale bars = 500 µm. PAG: Periaqueductal gray. **D)** A random sample of cell positions registered to the CCF atlas from each projection target shows an ordered trend along the SC polar axis, where Θ = 0° represents the ventral border of the SC and Θ = 90° represents the midline. Cells located between -3.8 and -4.3 posterior to bregma are binned and projected onto the CCF atlas at bregma: -4.05. Large dots show the centroid of each HVA-projecting input sample. **E)** Probability distribution function of theta distributions estimated using a kernel smoothing function with [0 90] boundary correction.

The pulvinar relays multimodal information to visual cortex

The cerebral cortex is the largest source of input to the pulvinar, and this input originates from a wide range of sensory, association, and frontal regions. We find, unsurprisingly, that the plurality of this input is visual, followed by retrosplenial (RSP), somatosensory (SS), motor, and auditory (AUD) input (Fig 1.4 A). When considering the functional significance of these CT inputs, the distribution of L5 "driving" cells will reflect the information that is likely to be relayed. We classified cortical inputs into layers based on their locations relative to the boundaries of a L5 marker, Ctip2 (Fig 1.4 C). Consistent with the reported convergence for these two CT cell types, we observed nine times more L6 inputs than L5. All HVA-projecting groups receive the most L5 input from V1. Interestingly, PM-projecting pulvinar neurons received almost as much driving input from RSP as from V1. RSP is an association area which occupies a higher position than extrastriate cortex in the visual hierarchy. RSP L5 input was substantial for all other cortical targets as well, so this pathway could be an interesting deviation from the canonical model depending on the pulvinar cell types involved. Multisensory input to the pulvinar was dependent on cortical target. LM- and PM- projecting neurons received very little input from SS and AUD cortex; and these inputs were relatively high for projections targeting AL, RL, and AM. Motor input to the pulvinar is preferentially routed to medial cortical targets AM and PM.

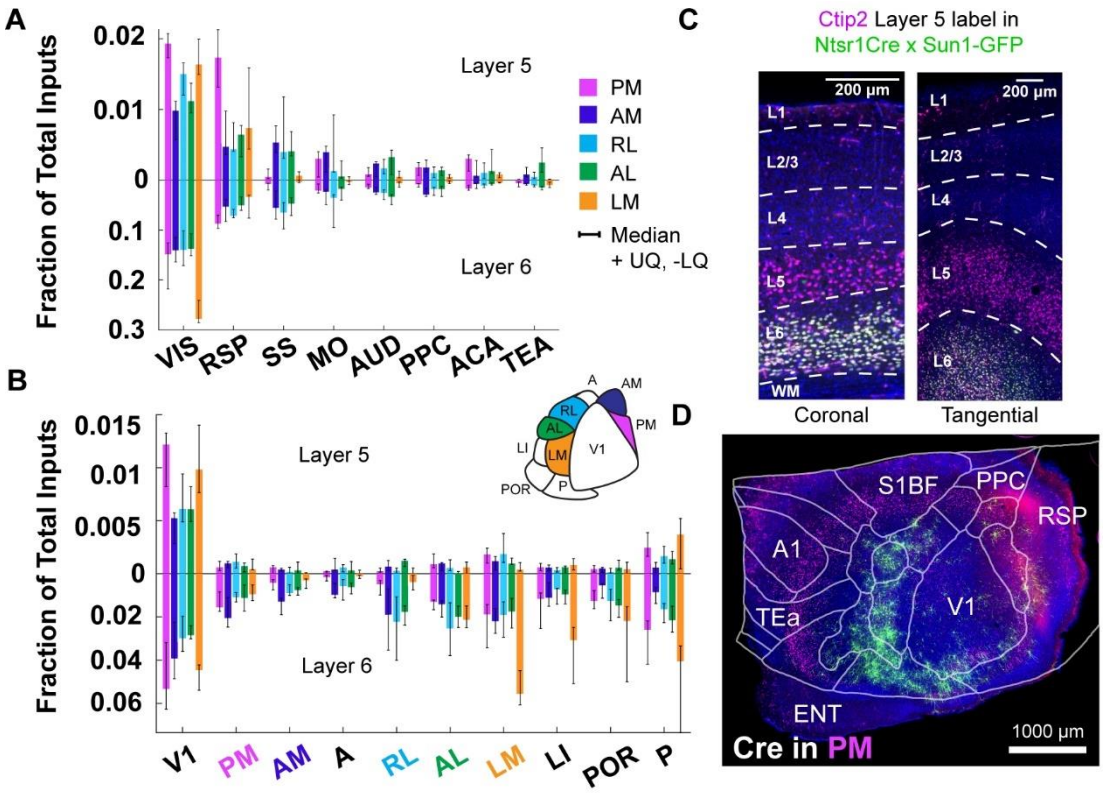

Figure 1.4 Cortico-pulvino-cortical pathways are organized like a feedforward relay. A) Major cortical inputs to the pulvinar from layer 5 (top axis) and layer 6 (bottom axis) expressed as the fraction of total inputs. Bar lengths correspond to the median values from each target area, with upper and lower quartile error bars. VIS: visual cortex; RSP: retrosplenial cortex; SS: somatosensory cortex; MO: motor cortex; AUD: auditory cortex; PPC: posterior parietal cortex; ACA: Anterior cingulate area; TEA: temporal association areas. **B)** Layer 5 (top axis) and layer 6 (bottom axis) inputs from V1 and nine HVAs. **C)** Immunohistochemical labeling of Ctip2 in a mouse expressing nuclear GFP in layer 6. Ctip2 (magenta) defines a band of lower layer 5 cells confirmed in coronal sections (left), and present in tangential sections (right). Scale bars = 200 µm. **D)** Example tangential cortical section showing GFP+ inputs to a PM-projecting starter population. Pulvinar axons (red) project to middle layers of medial HVAs. Ctip2 (magenta) defines a ring of layer 5. Visual area boundaries from ISI are aligned with cortical sections and merged with the CCF flatmap boundaries of nonvisual areas. Scale bar = 1000 µm. ENT: entorhinal cortex; TEa: temporal association area; A1: primary auditory cortex; S1BF: primary somatosensory barrel field; PPC: posterior parietal cortex; RSP: retrosplenial cortex; V1: primary visual cortex.

Transthalamic pulvinar connections reflect hierarchical relationships between visual areas

Further separating visual input by area revealed a striking difference in driving input from V1 and HVAs. Regardless of the downstream target, driving input was dominated by V1 projections, mirroring the feedforward corticocortical pathways from V1 to HVAs. Additional L5 inputs to other HVA-projecting populations were found in area P and LM. Corticocortical projections would position area P at a higher level than other HVAs in a cortical hierarchy[2], but methods to define this area vary and require further study. LM provided L5 input to all other HVA-projecting pulvinar groups, which aligns with its position as a V2-like structure in the corticocortical network. Modulating L6 inputs were more distributed than drivers, but most cells were still found in V1. Lateral HVAs provided more overall L6 input to the pulvinar than did medial HVAs.

For input/output relationships among HVAs, both L5 and L6 inputs demonstrated significant associations with the target area, indicating that these inputs are not generalized for all projection targets (L5: $p = 0.0000$, Fisher's exact test with Monte Carlo simulation; L6: $\chi^2 = 1.0 \times 10^3$, $p = 9.6 \times 10^{-190}$, Pearson's χ^2 test of independence). Further inspection of projection-specific input distributions revealed complementary organization of L5 and L6 inputs from HVAs. L5 inputs were rarely seen near the target area, but L6 cells were concentrated near the injection site (Fig 1.5A) With the exception of area PM, reciprocal connections from L6 were overrepresented compared to a null distribution of inputs (Fig 1.6C). L5, however, rarely made reciprocal connections back to its pulvinar projection neurons (Fig 1.6 B). Comparison of layer 5 reciprocal connections to the shuffled distribution revealed that AL- and LM- projecting neurons received statistically fewer reciprocal inputs than would be observed by chance. PM-, AM-, and RL-projecting reciprocal inputs were not statistically different than the shuffled distribution.

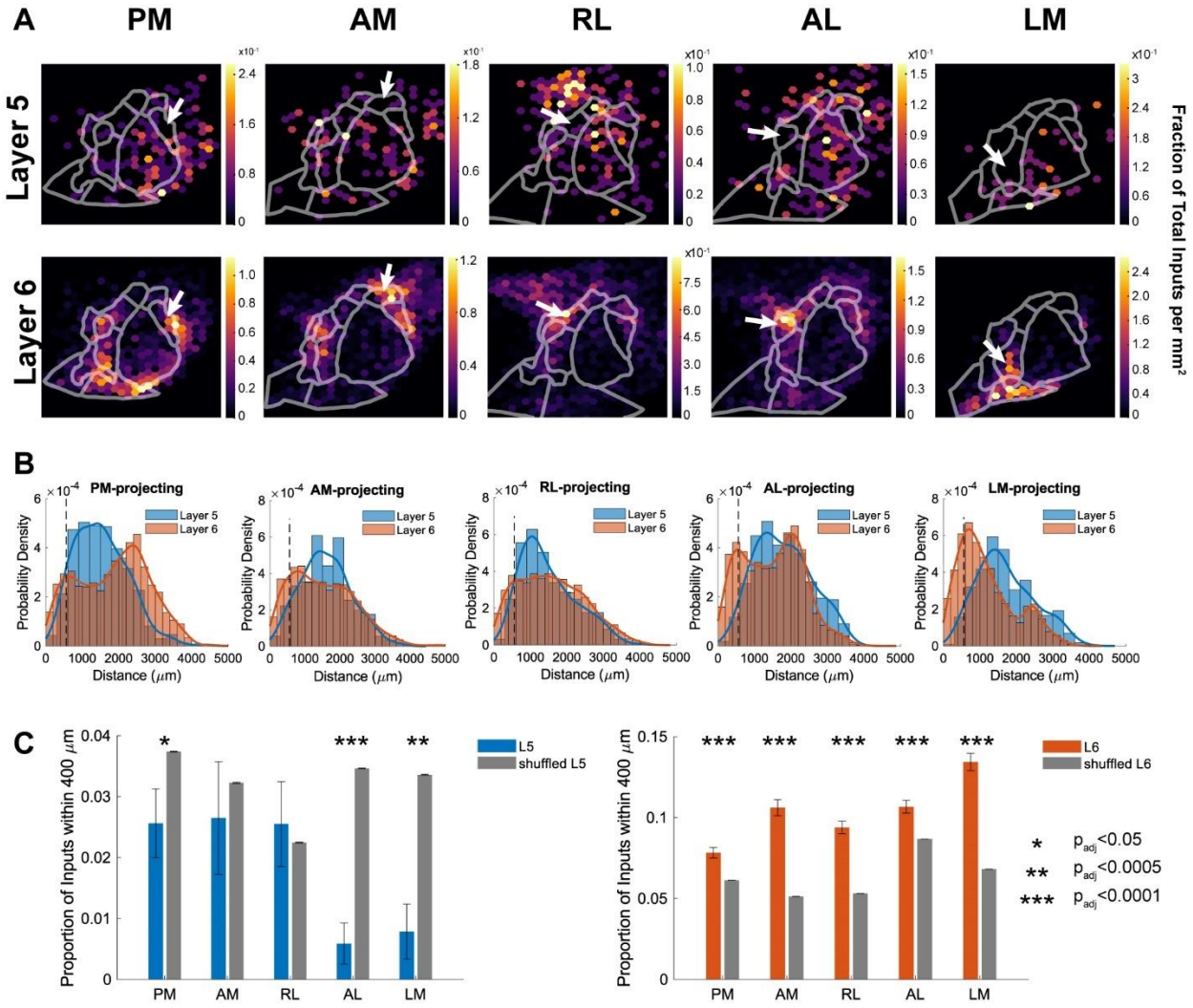

Figure 1.5 Distributions of input locations depend on layer and target area. A) Density of inputs to HVA-projecting pulvinar neurons from L5 (top) and L6 (bottom). **B)** Probability density of input distances from the injection site for L5 (blue) and L6 (orange) cells. Average radius of the injected HVA is denoted by the black, dashed, vertical lines. **C)** Proportion of inputs within 400 μm of the injection site compared to a distribution of 10^4 randomly shuffled targets. Error bars represent the standard error of the proportion. L5 inputs near the injection site were significantly lower than chance for areas PM ($\Delta\hat{p}$ = -0.0118±0.006 $SE_{\Delta p}$; p_{adj} = 0.0380), AL ($\Delta\hat{p}$ = -0.0287±0.003 $SE_{\Delta p}$; p_{adj} = 0.000), and LM ($\Delta\hat{p}$ = -0.0257±0.005 $SE_{\Delta p}$ p_{adj} = 0.0013), Benjamini-Hochberg FDR correction. L6 inputs near the injection site were significantly higher than the null distribution for all target areas (PM: $\Delta\hat{p}$ = 0.0171±0.003 $SE_{\Delta p}$; AM: $\Delta\hat{p}$ = 0.0548±0.005 $SE_{\Delta p}$; RL: $\Delta\hat{p}$ = 0.0408±0.004 $SE_{\Delta p}$; AL: $\Delta\hat{p}$ = 0.0200±0.004 $SE_{\Delta p}$; LM: $\Delta\hat{p}$ = 0.0662±0.005 $SE_{\Delta p}$; all p_{adj} = 0.000, Benjamini-Hochberg FDR correction)

When present, L5 reciprocal HVA inputs were typically only one or two neurons, so connections by area are highly sensitive to any small deviations in HVA borders or alignment. To investigate the anti-reciprocal L5 trend with a more robust measure, we analyzed the continuous spatial distributions of inputs (Fig 1.5B-C). Compared to a distribution of cells with shuffled target areas, L5 inputs were significantly less likely to be found within 400 μm of the injection site for areas PM, AL, and LM. RL and AM were not significantly different than the shuffled distribution. L6 inputs, conversely, were statistically more likely to be found near the injection site for all target areas. Together, these findings support the theory that the higher-order thalamus serves as a feedforward relay between cortical areas, and that both tectal and cortical input is dependent on the target of pulvinar relay cells.

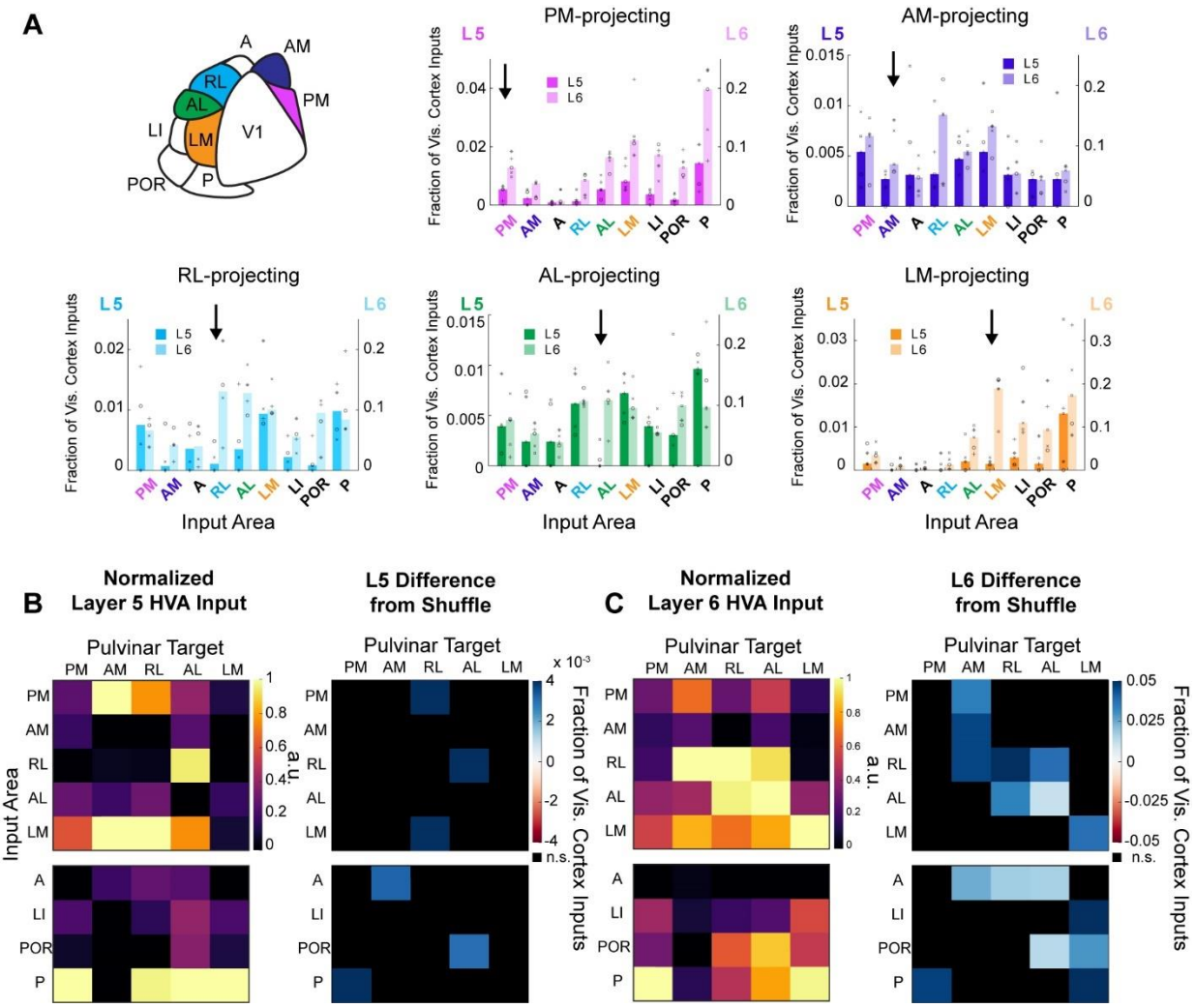

Figure 1.6 Complementary projection-specific relationship between L5 and L6 HVA inputs. A) Higher visual area inputs to each pulvinar projection population from L5 (dark bars, left axis) and L6 (light bars, right axis). Inputs are expressed as a fraction of visual cortical inputs. Arrows denote reciprocal connections. **B)** Left: Relative strength of input/output connections for L5. Median input proportions (rows) are normalized to the maximum for each target (columns). The upper matrix for each layer shows inputs from traced areas, where reciprocal connections lie along the diagonal. The lower matrices show additional inputs from non-injected HVAs. Significant associations exist between input area and target for L5 counts ($p = 0.0000$, Fisher's exact test). Right: Comparison of each L5 connection to a shuffled distribution of cells. Most comparisons are not significant ($p_{adj}>0.05$ with Benjamini-Hochberg FDR correction). **C)** Same as in (B) for L6. A significant relationship exists between input and target areas for L6 counts ($\chi^2 = 1.0 \times 10^3$, $p = 9.6 \times 10^{-190}$, Pearson's χ^2 test of independence). Compared to a shuffled distribution, reciprocal connections for target areas AM ($\Delta\mu = 0.0459$; $p_{adj} = 0.0000$), RL ($\Delta\mu = 0.0574$; $p_{adj} = 0.0000$), AL ($\Delta\mu = 0.0119$; $p_{adj} = 0.0127$), and LM ($\Delta\mu = 0.0377$; $p_{adj} = 0.000$) are significantly greater than chance. p-values adjusted with Benjamini-Hochberg FDR correction.

DISCUSSION

The pulvinar nucleus of the thalamus is a highly connected node of the visual network in the mammalian brain, and it can route incoming sensory signals to the cortex independently from the geniculate pathway[30,31]. While behavioral studies have demonstrated a role for the pulvinar in coordinating the activity of cortical areas, the fine-scale anatomical connections that underlie this function are not well described. In this study, we mapped the input/output connections of the mouse pulvinar with five HVAs using projection-specific, cre-dependent, monosynaptic, rabies tracing. We found that CT "drivers" and "modulators" follow distinct, but complementary, connection rules in the higher-order thalamus that resemble those governing the CT connections to the first-order dLGN. We also demonstrate a disynaptic pathway from both sensory and motor layers of the SC to all HVAs in the mouse.

Corticothalamocortical pathways have been proposed as parallel routes for signal transmission between cortical areas[3,32–35]. Such a transthalamic relay would require driving CT projections to make synaptic connections with driving thalamocortical relay cells that target downstream cortical areas. Several recent studies have confirmed such connections between V1 and areas AL and PM[17], as well as between the visual cortex and the ACA[26]. Similar higher-order transthalamic circuits through POm have been found between S1 and S2 and between S1 and M1[36,37]. These individual connections strongly suggest that feedforward transthalamic relays are a general organizational feature of hierarchical cortical networks, but until now there has not been a comprehensive map of input/output connections across an entire network. We found that L5 inputs to thalamocortical relay cells projecting throughout the visual cortical network predominantly originate from V1 (Fig 1.7A), thus establishing that parallel, transthalamic relays are indeed a universal organizational principle. We found a high ratio of L5 inputs from V1

compared to HVAs for all target areas. Leow et al. traced the inputs to pulvinar projections targeting the ACA, which is near the top of the visual hierarchy; interestingly, they find more L5 inputs from HVAs than from V1, suggesting that the L5 distribution reflects hierarchical relationships rather than trivial factors such as area size[26]. Additional input/output tracing of pulvinar projections to areas TEa, RSP, and other higher-order sensory cortices could reveal potentially interesting pathways from HVA L5 cells. The signals conveyed by transthalamic pathways are distinct from corticocortical signals[17], and they originate from collaterals of L5b axons that target subcortical motor centers[34,35,38]. Understanding the nature of this message and how it might interact with the direct corticocortical stream is an essential goal of thalamocortical research.

A surprising source of L5 input to HVA-projecting pulvinar cells was RSP. RSP was the next largest source of L5 input after V1, and these inputs were greater than from any HVA. RSP is typically considered to be at a higher level of the visual hierarchy than HVAs based on corticocortical connections, but this thalamic connectivity would place RSP at a lower level. The ratio of L5 inputs to L6 inputs was relatively higher for RSP than other sensory areas, which aligns with another recent study that analyzed projection volumes from RSP to the pulvinar[10]. Under freely moving conditions, more than half of L5 neurons in RSP encode signals related to head velocity[39], so this L5 pathway from RSP could play an important role in shaping the self-motion signals present in the pulvinar[40]. RSP L5 extratelencephalic (ET) neurons have unique transcriptional profiles compared to the rest of the neocortex[41], and many of them have additional cortico-cortical branches[42]. Given these deviations from the typical L5 ET cell type features, RSP L5 corticothalamic terminals could potentially have distinct synaptic properties

from typical drivers. Electrophysiological characterization of the RSP→Pulvinar connections could clarify the nature of this transthalamic pathway.

Compared to L5 inputs from V1, HVA L5 inputs were rare. However, comparison of L5 inputs *between* HVAs revealed a significant absence of reciprocal connections for 3 of the 5 target areas studied. This finding provides direct support for the "no-strong-loops" hypothesis, which asserts that there should be no reciprocal connections with strong synaptic weights in both directions[28]. While the L5 CT projections are "strong", we do not yet have a way to experimentally separate the two classes of TC relay cells in the mouse. The pulvinar contains a mix of core and matrix cells[11,13,43,44], and only the former would constitute a "strong" projection. Projections from the pulvinar to HVAs are predominantly "core" type[15,43–45], but the relative core and matrix projections to HVAs varies with pulvinar subdivision[13]. Reciprocal connections from L5 that we do find for areas RL and AM could be inputs onto matrix cells from the rostromedial pulvinar, so these results do not necessarily violate the "no-strong-loops" hypothesis. In fact, input/output tracing of V1-projecting pulvinar neurons, which are exclusively matrix-type, does identify significant reciprocal L5 inputs[14]. Developing genetic access to core and matrix cells in the rodent would allow us to specify the connectivity of CT inputs to the two different classes of TC output and would greatly advance the study of thalamocortical function.

Given the difference in magnitude between driving input from V1 vs HVAs, the lack of reciprocal L5 connections to HVAs is unlikely to have a strong influence on the overall activity of TC projections. However, the specificity in wiring required to avoid reciprocal connections is an interesting developmental phenomenon. L5 and L6 axon terminal fields from a given cortical area are highly overlapping[23], so the absence of L5 reciprocal connections cannot be due to differential spatial distribution of terminals. The guidance of L5 and L6 axons into thalamic

nuclei in early development involves a highly complex sequence of structural and molecular cues, and depends intimately on the coordination of ascending TC axons and descending subplate projections[46]. Our results suggest that in addition to these signals guiding CT axons to their target nuclei, there may be additional signaling mechanisms at the level of individual TC core cells that prevent or prune reciprocal synapse formation for L5 axons.

Input/output tracing of pulvinar projections to areas PM and AL in a previous study reported feedforward L5 pathways, but did not find a significant lack of reciprocal connections[17,26]. We believe this difference can be attributed to two technical factors related to viral targeting and optimization. In our control experiments with no glycoprotein, we found that AAV-FLEX-TCB at high titers caused significant retrograde infection of L5 neurons in the target area. Since the overall number of L5 inputs is low, this target-specific artifact would nullify the true anti-reciprocal distribution. Additionally, injections of AAV-Cre that spread across areas can result in labeling of L5 inputs from both HVAs that might target the other, as we observed for injections at the P/POR border.

L6 cells comprised 90% of the total inputs to pulvinar projections. Accordingly, we found that their distribution did align with the topography of broader input/output correlations found with bulk tracing[23]. Namely, reciprocal connections were more likely than chance for L6 inputs, but inputs were found across visual areas with a characteristic distribution (Fig 1.7B). We found that this distribution was highly sensitive to the spread of helper viruses in the pulvinar, and that biased or incomplete coverage of projection fields resulted in similarly biased cortical input sampling. L6 reciprocal connections may be even more pronounced in the primate, where the topography of corticothalamic projections is more segregated than in the rodent pulvinar. Functional studies have shown that L6 modulating inputs do not meaningfully influence the

receptive field content of thalamic neurons, but they are capable of inhibiting thalamic activity through their collaterals to the TRN and controlling the gain and frequency of thalamic responses[25,47–50]. Most of these effects have been described for L6 feedback to first-order thalamic nuclei. Evidence shows that these modulatory influences are similar for the pulvinar, but our results demonstrate that the sources of L6 modulation are much more diverse than for corticogeniculate feedback. Broad L6 modulation to all pulvinar projections could be one mechanism supporting the synchronization of cortical areas by the pulvinar.

Most retinal input reaches the cortex through the dLGN; however, the pulvinar provides a secondary pathway for incoming retinal signals via the superficial SC[7,31,51–54]. This pathway is important for the development of the cortex[55,56], and it can support "blindsight", wherein some visually-guided actions remain intact after lesions to the striate cortex[57–64]. We found that all HVAs in the mouse receive disynaptic input from the SC, which is a notable deviation from the highly specialized primate circuitry, where this pathway is unique to dorsal visual areas[7]. While the framework of dorsal and ventral pathways has been highly influential in the study of primate visual cortex[65–69], the classification of two distinct visual streams in the mouse is less clear[2,4,54,69,70]. Our results suggest that tectal input may be more relevant to the mouse cortex than previously thought, and that all mouse HVAs have some degree of connectivity resembling the primate dorsal pathway from SC. SC inactivation slightly alters visual responses in many HVAs[22], but to distinguish between the role of direct SC input and interactions between cortical areas, additional studies combining striate and SC inactivation are necessary[30,71,72]. SC inputs are not uniform, however, as we found a much stronger superficial SC projection to LM than other areas. The SC inputs to LM are probably undersampled because our injections often did not fully cover the caudal pulvinar, which receives extensive inputs from the superficial SC[6].

The SC projection to the mouse pulvinar is primarily from motion-sensitive widefield vertical cells in the superficial SC[6,73]. In addition to these well-described inputs, we also identified a smaller, but significant input from deep SC to all HVAs, particularly from the intermediate gray layer. These inputs are present, but less numerous in other bulk tracing studies[23,29], and they are consistent with deep SC inputs labeled with transsynaptic tracing[17]. Cells in these layers carry the motor output signals of the SC, but their influence on thalamocortical activity is unknown.

In summary, we have generated a comprehensive input/output map of the mouse pulvinar which extends the principles of first order corticothalamic connectivity into the higher-order nuclei. Our data confirm long-standing theories that driving CT inputs are feedforward relays and avoid reciprocal loops[3,28]. Moreover, we have described tectal input to the pulvinar that targets all cortical areas. These findings support the distinction of direct and transthalamic pathways between cortical areas, but additional research is necessary to investigate the functional roles for these circuits in visual behaviors and cortical activity.

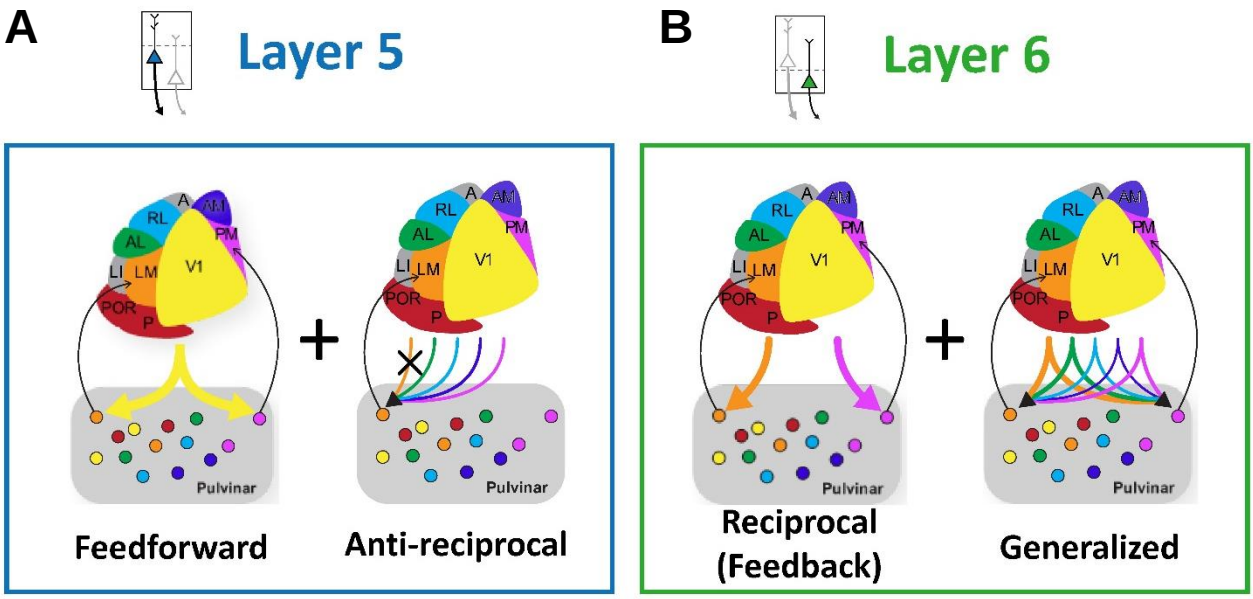

Figure 1.7 Summary of Input/Output Connections in the Pulvinar. A) Schematic showing connections of L5 CT projections with the pulvinar. Inputs from L5 drivers are feedforward and anti-reciprocal. **B)** Schematic showing L6 CT connections with the pulvinar. L6 modulators follow a general distribution with increased input from lateral HVAs, with an additional reciprocal component for each target area.

METHODS

Animals

Twenty-four Adult female and male C57BL/6J mice (The Jackson Laboratories) aged 6-10 weeks were used in this study. All experimental procedures followed procedures approved by the Salk Institute Animal Care and Use Committee.

Viruses

AAV5-Ef1α-Cre-WPRE (UNC Vector Core)

AAV8-CAG-FLEX-TCB ($2.04x10^{13}$ GC/mL; Salk GT3 Core)

AAV8-CAG-FLEX-oG-WPRE-SV40pA ($1.55x10^{13}$ GC/mL; Vigene Biosciences)

EnvA+RVdG-eGFP ($3.29x10^{8}$ TU/mL; Salk GT3 Core)

Surgical Procedures

To trace the inputs to specific projection populations, a mixture of AAV8-CAG-FLEX-TCB and AAV8-CAG-FLEX-oG-WPRE-SV40pA was injected into the pulvinar. To prevent glycoprotein-independent retrograde labeling of CT neurons, AAV8-CAG-FLEX-TCB was diluted to between $8.16x10^{11}$ - $4.04x10^{12}$ GC/mL with Hank's Buffered Saline Solution, then mixed in a 1:1 ratio with AAV8-CAG-FLEX-oG-WPRE-SV40pA. In control experiments with no AAV-oG [74], higher concentrations of AAV-TCB resulted in non-specific RVdG-eGFP expression in layer 5b and layer 6 of cortex, restricted to the location of the AAV5-Cre injection site. At the optimized TVA concentration, RVdG-eGFP+ neurons were observed locally at the pulvinar injection site, but not in the cortex or any other distal structures. We frequently saw a small number of GFP+ astrocytes at the AAV-Cre injection site, usually in upper cortical layers and with distinct morphology. These were present regardless of AAV-TCB concentration and were not counted in the experimental brains. Control injections without Cre but including

glycoprotein did not result in any long-range labeling, even at the higher TVA concentrations which failed the no-glycoprotein control.

Mice were anesthetized with isoflurane (2% induction; 1.5% maintenance) and mounted in a stereotax (David Kopf Instruments Model 940 series). Using a carbide burr, a small craniotomy was made over the left pulvinar (-1.8 to -2.3 from bregma; -1.2 to -1.6 lateral from the midline). Injection coordinates varied depending on the cortical projection region. The virus was pressure-injected via syringe at a rate of 10 nL/min through a tapered glass pipette (25-30 μm tip inner diameter) at a depth of 2.3-2.5 mm below the pial surface. To prevent backflow of the virus into the hippocampus and cortex, the pipette was left in place for at least 10 minutes before retraction. During the same surgery, a custom metal headframe was attached to the skull with dental cement (C&B Metabond, Parkell) as previously described[75]. Either buprenorphine-SR (0.5-1 mg/kg) or meloxicam (4 mg.kg) were administered subcutaneously for post-op analgesia. Mice recovered for 1-4 days in their home cage with a suspension of ibuprofen (30 mg/kg) in water prior to intrinsic signal imaging (ISI).

After ISI mapping, blood vessel landmarks were used to target injections of AAV5-Ef1α-Cre-WPRE to one of six HVAs (PM, AM, RL, AL, LM, or P/POR). We chose AAV5 for its high propensity to infect long-range thalamocortical axons. In comparison, AAVretro-Cre caused marked toxicity and reduced cell labeling at the cortical injection site, and when diluted to nontoxic concentrations, it was comparably efficient to AAV5-Cre. The virus was injected via syringe as described above at two depths between 200-500 μm below the pial surface. The total volume of AAV-Cre ranged between 35-75 nL and was chosen based on the size of each HVA to maximize coverage without spreading into adjacent visual areas as confirmed by AAV-Cre injections into Ai14 mice. The skull thinning required for ISI is appropriate for short survival

times but leads to infection and tissue degradation after approximately a week. Due to the long survival time required for expression of oG, we removed the skull after thinning and placed a molded cement cover over the craniotomy to preserve the tissue health. A subset of animals was imaged without any skull thinning to guide injections, and then subsequently imaged more thoroughly with thinning in the days prior to euthanasia.

Three weeks after injection of AAV-Cre, 350 nL of EnvA+RVdG-eGFP was injected into the pulvinar at the previous site at 2-3 depths between 2.3-2.6 mm below the pial surface. Buprenorphine-SR (0.5-1 mg/kg) was administered subcutaneously, and mice received ibuprofen in their water (30 mg/kg) as they recovered in their cages for 10 days until tissue harvesting.

Intrinsic Signal Imaging

After viral injections in the thalamus, higher visual areas (HVAs) in cortex were identified using intrinsic signal imaging (ISI) through a thinned skull as previously described [9,75]. Mice were anesthetized with 0.1-1% isoflurane and sedated with (1 mg/kg) chlorprothixene hydrochloride injected intramuscularly. Anesthesia was continuously monitored and adjusted to maintain a lightly anesthetized state (1-1.5 breaths/second). Most experiments resulted in maps with seven visual areas (V1, PM, AM, RL, AL, LM, and P/POR) successfully segmented. These maps were used to guide cortical injections and to align post-mortem tissue to the HVA borders. Occasionally, the initial map of visual cortex identified a subset of these areas. In these cases, the partial map was sufficient to target a cortical injection, and ISI was repeated just prior to the experimental endpoint with a more thoroughly thinned skull for a full map that was suitable for post-mortem tissue alignment. The border between P and POR was usually ambiguous, so these injections were targeted generally to the positive field sign area directly behind LM, which likely included both areas. Due to this ambiguity, only PM, AM, RL, AL, and LM injections were

included in this study.

Histology

Mice were euthanized with an intraperitoneal injection of Euthasol (15.6mg/ml), then transcardially perfused with phosphate-buffered saline (PBS) followed by 4% paraformaldehyde (PFA). After dissection, brains were post-fixed in 2% PFA and 15% sucrose in PBS for 16-24 hours at 4°C, then submerged in 30% sucrose for an additional 16-24 hours at 4°C.

The left visual cortex and hippocampus were dissected from the rest of the brain and sectioned tangentially on a freezing microtome. After making the first 250 μm section which contained the surface blood vessels, the remaining cortical tissue was sectioned in 50 μm increments. Immunohistochemical staining of the free-floating cortical sections amplified the eGFP and mCherry signals and provided a laminar marker to distinguish layer 5 from layer 6. After blocking at room temperature in PBS with 10% normal donkey serum (NDS) and 0.5% Triton-X, tissue was incubated for 16 hours at 4°C with goat anti-GFP (1:500; 600-101-215; Rockland Immunochemical), rabbit anti-dsRed (1:500; 632496; Takara Bio USA), and rat anti-Ctip2 (1:1000; ab18465; Abcam) in PBS with 1% NDS and 0.5% Triton-X. The tissue was then incubated for 6 hours at room temperature with donkey anti-goat conjugated to Alexa Fluor 488 (1:500; A-11055; Thermo-Fisher), donkey anti-rabbit conjugated to Alexa Fluor 568 (1:500; A-10042; Thermo-Fisher), and donkey anti-rat conjugated to Cy5 (1:500; 712-175-153, Jackson ImmunoResearch) in PBS with 1% NDS and 0.5% Triton-X, followed by a counterstain with 10 μM DAPI in PBS. Tangential sections were mounted on gelatin-subbed slides, air-dried, then coverslipped with polyvinyl alcohol mounting medium containing 1,4-diazabicyclo-octane (PVA-DABCO).

The remaining brain tissue was sectioned coronally on a freezing microtome in 50 μm

increments from the olfactory bulb to the end of the cerebellum. Free-floating sections were blocked in PBS with 5% NDS and 1% Triton-X for 1 hour at room temperature, then incubated with goat anti-GFP (1:500; 600-101-215; Rockland Immunochemical) and rabbit anti-dsRed (1:500; 632496; Takara Bio USA) in PBS with 1% NDS and 0.5% Triton-X for 16-24 hours at 4°C. The tissue was then incubated in the appropriate secondary antibodies for 2 hours at room temperature, then counterstained with DAPI. Coronal sections were mounted on glass slides with PVA-DABCO.

Image Processing and Registration

All slides were imaged on an Olympus BX63 epifluorescence microscope with a 10X objective. Cells in coronal sections, were either counted manually and assigned to brain areas based on cytoarchitectonic landmarks by an expert, or counted manually and automatically registered to the Allen Common Coordinate Framework (CCF)[76] after transforming sections using the SHARP-TRACK program[77] and custom Matlab scripts. Medial TRN cells were sometimes mistakenly assigned to VPL due to slight misalignments at the nuclei border. Therefore, those cells were manually checked and compared to cytoarchitectonic landmarks. The percentage of cells assigned to major brain areas was comparable between these two registration methods.

Z-stacks of tangential cortical sections were processed in the Olympus cellSens software using the Extended Focal Imaging method, then converted for additional processing using ImageJ software (NIH). Cortical sections were virtually "flattened" using radial blood vessel alignment[78], which corrected for the curvature of the cortex and aligned cells in deep layers with the HVA assignments defined at the pial surface. This alignment was achieved with sequential affine matrix transformations of deeper sections onto superficial sections using the Landmarks

Registration plugin. When apical dendrites could be matched between images, they were included as landmarks in addition to radial blood vessels. The anatomical reference and HVA border map obtained during ISI were similarly warped onto the aligned image stack using common surface blood vessel landmarks present in the top tangential section. Cells in each transformed section were registered to the aligned HVA map and assigned to a cortical layer based on the borders of the Ctip2 signal in individual sections. The retinotopically organized, positive field sign patch designated as RL usually extended into the S1 barrel field as has been previously reported [79], so the anterior border was modified from the automatically segmented borders so that it aligned with the posterior edge of the imaged S1 barrel fields. All RL injection sites were still contained within the truncated borders. Area A lies in between RL and AM [8,9], but was never segmented in our ISI. The medial border of RL was therefore estimated to lie along a line extending from the gamma barrel in between rows C and D to V1. Although the definition of area A and AM relative to the posterior parietal cortex (PPC) is still currently under debate[80,81], we defined A as the region between RL and AM which is visually responsive and retinotopically organized. The area outside of these functional borders and posterior to somatosensory cortex was defined as PPC.

Input cells were frequently labeled in the nonvisual areas contained in tangential sections. To assign these areas, we used the 3D volume created from the coronal sections to define the edges of the dissected region in the Common Coordinate Framework (CCF). This dissection boundary was then mapped onto the CCF flatmap, which was aligned to the cut edges of the tangential stack.

Visual areas P and POR were only partially mapped by intrinsic signal imaging due to these areas extending behind the lambda suture and laterally out of the imaging ROI in the case

of POR. The anterior borders with LM and V1 were confirmed with ISI mapping, but the remaining boundaries of POR were defined by the transformed flatmap and the border of the entorhinal cortex which was evident from the cytoarchitecture. We observed a positive field sign band extending behind V1 as has been reported previously[79]. In post-mortem tissue, this region frequently had TVAmCherry^{+} pulvinar axons in layer 4, which confirms that this area is a separate region from V1, which only receives matrix projections to layer 1 and 5a[15]. Rather than defining the whole posterior edge of the cortex as area P, we used the most lateral edge of the dense DAPI band in RSPv layer 2/3 to delineate the border between P and RSP.

Exclusion Criteria

Since the pulvinar is topographically organized with respect to its cortical inputs and outputs, the accuracy of targeting for both helper virus injection and the RVdG injection was crucial to avoid biasing the measured input samples. Animals were excluded if the two injections did not overlap, in which cases we observed reduced starter cell populations and little to no transsynaptic labeling. We excluded animals whose starter cell locations were restricted or heavily biased to the tectal-recipient caudal Pulvinar, as the corresponding cortical inputs were either absent or only present in caudally-projecting area POR. We also excluded animals whose starter cells were biased compared to the overall distribution of starter cells for a given projection population, which aligned with the topographical organization that has been previously reported[16,23]. We excluded experiments for which surface blood vessels could not be accurately aligned. This was rare when the quality of the craniotomy and coverslip placement was good. While we injected at least 6 mice that met these criteria for areas P and POR, our injections were not restricted to the individual areas and instead covered both P and POR. Due to this ambiguity in cortical target, these experiments were also excluded from analysis.

Analysis and Statistical Methods

Because the glycoprotein was not labeled with a fluorescent marker, we considered any GFP+ cell near the injection site to be a starter cell. All other cells were classified as inputs and expressed as a fraction of the total population of inputs for each brain region (total inputs summarized in Table 1.S1). Brain-wide inputs to each projection population were compared with a Kruskal-Wallis test, with post-hoc Dunn-Šidák correction for significant comparisons.

To compare the relative positions of SC inputs to different projection populations, cell positions from one example experiment per target were registered to the CCF using the forward transforms obtained from tissue registration described previously. Because the total number of inputs varied between animals, 166 cells were randomly subsampled from each animal to generate distributions which did not vary based on the tracing efficiency or SC input percentage. These cells were binned into four divisions extending across the anterior/posterior extent of SC and plotted with the atlas boundaries obtained at the center of each bin. One example bin is displayed in Fig 1.3(d).

Previous work has described a systematic organization of SC inputs and outputs that varies along the radial extent of SC[29]. To determine whether the SC inputs to pulvinar shared this trend for cortical topography, we defined an angle, theta (Θ), representing cell positions along a polar axis where the ventral boundary of the SC bin is 0° and the midline is 90°. Probability density functions were fit to the theta values for the full samples of SC cells using a kernel smoothing function with boundary correction at 0° and 90°.

Layer 5 and layer 6 density maps were generated by binning the continuous distributions of cell positions for each animal in hexagonal bins with a width of 180.6 μm. Example brains for each target area are shown. Cartesian distances of input cells to the injected area were calculated

from the transformed tissue. Distances of all cells from each target area were fit with a kernel smoothing function to estimate the probability density.

A null distribution of cell distances was generated by shuffling the target area 10,000 times and recalculating the cell distances from the shuffled target locations. To test whether observations of layer 5 or 6 cells near the injection site were different than would be observed by chance, we compared the true proportion of cells within a 400 μm radius to the proportions calculated from the shuffled distributions. We calculated one-tailed p-values for layer 5 and 6 to test for anti-reciprocity and reciprocity, respectively. P-values were adjusted using the Benjamini-Hochberg procedure for control of false discovery rate.

Outliers with large proportions of inputs in SC conversely had lower overall proportions of visual cortical input, so we normalized HVA inputs to the total visual cortical inputs for discretized area comparisons. Fractions of visual cortical input to each projection target were compared for layer 5 and 6. To visualize the relative strengths of these HVA connections, we plotted the median input values in a heatmap. Color scales normalized for each target area (column), resulting in a visualization of the relative strengths of each input compared to the strongest input, in arbitrary units.

To test for significant input/output associations for layer 5 connections, we performed a fisher's exact test on the raw cell counts with monte carlo simulation (9.6×10^7 shuffles) to a estimate a p-value ±0.0001 with 95% confidence. Layer 6 sample sizes were much higher than layer 5, so a Pearson's χ^2 test for independence was applied to the layer 6 input/output matrix. The shuffling procedure for cell distances was repeated for the cells' HVA assignments to generate a null distribution of area counts to compare against projection-specific distributions.

APPENDIX

Table 1.S1 Summary of total inputs

PM		AM		RL		AL		LM	
ID	No. of Inputs	ID	No. of Inputs	ID	No. of Inputs	ID	No. of Inputs	ID	No. of Inputs
V07	7710	V48	1531	V53	5762	V49	8874	V08	2595
V55	4562	V81	5182	V59	9173	V65	2957	V27	1670
V61	2870	V96	1707	V73	972	V97	3273	V30	2373
V63	1663	V106	2585	V102	2401	V98	2187	V56	2444
V75	4505	V108	2053			V99	4258	V64	3069

ACKNOWLEDGEMENTS

Chapter 1, in full, is currently being prepared for submission for publication and will include Angel Macias, Will N. Lagos, and Genevieve Ugorji as co-authors and Professor Edward Callaway as the senior author. The dissertation author was the primary researcher and author of this material.

REFERENCES

1. Felleman, D. J. & Van Essen, D. C. Distributed hierachical processing in the primate cerebral cortex. *Cereb. Cortex* **1,** 1–47 (1991).

2. Wang, Q., Sporns, O. & Burkhalter, A. Network Analysis of Corticocortical Connections Reveals Ventral and Dorsal Processing Streams in Mouse Visual Cortex. **32,** 4386–4399 (2012).

3. Sherman, S. M. & Guillery, R. W. Distinct functions for direct and transthalamic corticocortical connections. *J. Neurophysiol.* **106,** 1068–1077 (2011).

4. Beltramo, R. & Scanziani, M. A collicular visual cortex: Neocortical space for an ancient midbrain visual structure. *Science* **363,** 64–69 (2019).

5. Allen, A. E., Procyk, C. A., Howarth, M., Walmsley, L. & Brown, T. M. Visual input to the mouse lateral posterior and posterior thalamic nuclei: photoreceptive origins and retinotopic order. *J. Physiol.* **594,** 1911–1929 (2016).

6. Zhou, N., Maire, P. S., Masterson, S. P. & Bickford, M. E. The mouse pulvinar nucleus: Organization of the tectorecipient zones. *Vis. Neurosci.* **34,** E011 (2017).

7. Lyon, D. C., Nassi, J. J. & Callaway, E. M. A Disynaptic Relay from Superior Colliculus to Dorsal Stream Visual Cortex in Macaque Monkey. *Neuron* **65,** 270–279 (2010).

8. Wang, Q. & Burkhalter, A. Area map of mouse visual cortex. *J. Comp. Neurol.* **502,** 339–357 (2007).

9. Garrett, M. E., Nauhaus, I., Marshel, J. H. & Callaway, X. E. M. Topography and Areal Organization of Mouse Visual Cortex. **34,** 12587–12600 (2014).

10. Harris, J. A., Mihalas, S., Hirokawa, K. E., Whitesell, J. D., Choi, H., Bernard, A., Bohn, P., Caldejon, S., Casal, L., Cho, A., Feiner, A., Feng, D., Gaudreault, N., Gerfen, C. R., Graddis, N., Groblewski, P. A., Henry, A. M., Ho, A., Howard, R., Knox, J. E., Kuan, L., Kuang, X., Lecoq, J., Lesnar, P., Li, Y., Luviano, J., McConoughey, S., Mortrud, M. T., Naeemi, M., Ng, L., Oh, S. W., Ouellette, B., Shen, E., Sorensen, S. A., Wakeman, W., Wang, Q., Wang, Y., Williford, A., Phillips, J. W., Jones, A. R., Koch, C. & Zeng, H. Hierarchical organization of cortical and thalamic connectivity. *Nature* **575,** 195–202 (2019).

11. Jones, E. G. Viewpoint: the core and matrix of thalamic organization. *Neuroscience* **85,** 331–345 (1998).

12. Phillips, J. W., Schulmann, A., Hara, E., Winnubst, J., Liu, C., Valakh, V., Wang, L., Shields, B. C., Korff, W., Chandrashekar, J., Lemire, A. L., Mensh, B., Dudman, J. T., Nelson, S. B. & Hantman, A. W. A repeated molecular architecture across thalamic pathways. *Nat. Neurosci.* **22,** 1925–1935 (2019).

13. Nakamura, H., Hioki, H., Furuta, T. & Kaneko, T. Different cortical projections from three subdivisions of the rat lateral posterior thalamic nucleus: a single-neuron tracing study with viral vectors. *Eur. J. Neurosci.* **41,** 1294–1310 (2015).

14. Miller-Hansen, A. J. & Sherman, S. M. Conserved patterns of functional organization between cortex and thalamus in mice. *Proc. Natl. Acad. Sci.* **119,** e2201481119 (2022).

15. Zhou, N., Masterson, S. P., Damron, J. K., Guido, W. & Bickford, M. E. The Mouse Pulvinar Nucleus Links the Lateral Extrastriate Cortex, Striatum, and Amygdala. *J. Neurosci.* **38,** 347–362 (2018).

16. Juavinett, A. L., Kim, E. J., Collins, H. C. & Callaway, E. M. A systematic topographical relationship between mouse lateral posterior thalamic neurons and their visual cortical projection targets. *J. Comp. Neurol.* **528,** 99–111 (2020).

17. Blot, A., Roth, M. M., Gasler, I., Javadzadeh, M., Imhof, F. & Hofer, S. B. Visual intracortical and transthalamic pathways carry distinct information to cortical areas. *Neuron* **109,** 1996-2008.e6 (2021).

18. Cappe, C., Morel, A., Barone, P. & Rouiller, E. M. The Thalamocortical Projection Systems in Primate: An Anatomical Support for Multisensory and Sensorimotor Interplay. *Cereb. Cortex* **19,** 2025–2037 (2009).

19. Froesel, M., Cappe, C. & Ben Hamed, S. A multisensory perspective onto primate pulvinar functions. *Neurosci. Biobehav. Rev.* **125,** 231–243 (2021).

20. Chou, X., Fang, Q., Yan, L., Zhong, W., Peng, B., Li, H., Wei, J., Tao, H. W. & Zhang, L. I. Contextual and cross-modality modulation of auditory cortical processing through pulvinar mediated suppression. *eLife* **9,** e54157 (2020).

21. Gattass, R., P.B. Sousa, A. & Oswaldo-Cruz, E. Single unit response types in the pulvinar of the cebus monkey to multisensory stimulation. *Brain Res.* **158,** 75–87 (1978).

22. Tohmi, M., Meguro, R., Tsukano, H., Hishida, R. & Shibuki, K. The extrageniculate visual pathway generates distinct response properties in the higher visual areas of mice. *Curr. Biol.* **24,** 587–597 (2014).

23. Bennett, C., Gale, S. D., Garrett, M. E., Newton, M. L., Murphy, G. J. & Olsen, S. R. Higher-Order Thalamic Circuits Channel Parallel Streams of Visual Information in Mice. 19

24. Shipp, S. The functional logic of cortico–pulvinar connections. *Philos. Trans. R. Soc. Lond. B. Biol. Sci.* **358,** 1605–1624 (2003).

25. Kirchgessner, M. A., Franklin, A. D. & Callaway, E. M. Distinct "driving" versus "modulatory" influences of different visual corticothalamic pathways. *Curr. Biol.* **31,** 5121-5137.e7 (2021).

26. Leow, Y. N., Zhou, B., Sullivan, H. A., Barlowe, A. R., Wickersham, I. R. & Sur, M. Brain-wide mapping of inputs to the mouse lateral posterior (LP/Pulvinar) thalamus–anterior cingulate cortex network. *J. Comp. Neurol.* **530,** 1992–2013 (2022).

27. Schwarz, L. A., Miyamichi, K., Gao, X. J., Beier, K. T., Weissbourd, B., DeLoach, K. E., Ren, J., Ibanes, S., Malenka, R. C., Kremer, E. J. & Luo, L. Viral-genetic tracing of the input–output organization of a central noradrenaline circuit. *Nature* **524,** 88–92 (2015).

28. Crick, F. & Koch, C. Constraints on cortical and thalamic projections: the no-strong-loops hypothesis. *Nature* **391,** 245–250 (1998).

29. Benavidez, N. L., Bienkowski, M. S., Zhu, M., Garcia, L. H., Fayzullina, M., Gao, L., Bowman, I., Gou, L., Khanjani, N., Cotter, K. R., Korobkova, L., Becerra, M., Cao, C., Song, M. Y., Zhang, B., Yamashita, S., Tugangui, A. J., Zingg, B., Rose, K., Lo, D., Foster, N. N., Boesen, T., Mun, H.-S., Aquino, S., Wickersham, I. R., Ascoli, G. A., Hintiryan, H. & Dong, H.-W. Organization of the inputs and outputs of the mouse superior colliculus. *Nat. Commun.* **12,** 4004 (2021).

30. Rodman, R., Gross, G. & Albrightb, D. Afferent Basis of Visual Response Properties in Area MT of the Macaque. II. Effects of Superior Colliculus Removal.

31. Petry, H. M. & Bickford, M. E. The Second Visual System of The Tree Shrew. *J. Comp. Neurol.* **527,** 679–693 (2019).

32. Guillery, R. W. Anatomical evidence concerning the role of the thalamus in corticocortical communication: a brief review. *J. Anat.* **187 (Pt 3),** 583–592 (1995).

33. Sherman, S. M. & Guillery, R. W. *Functional connections of cortical areas: a new view from the thalamus*. (MIT press, 2013).

34. Guillery, R. W. in *Prog. Brain Res.* **149,** 235–256 (Elsevier, 2005).

35. Guillery, R. W. Branching Thalamic Afferents Link Action and Perception. *J. Neurophysiol.* **90,** 539–548 (2003).

36. Theyel, B. B., Llano, D. A. & Sherman, S. M. The corticothalamocortical circuit drives higher-order cortex in the mouse. *Nat. Neurosci.* **13,** 84–88 (2010).

37. Mo, C. & Sherman, S. M. A Sensorimotor Pathway via Higher-Order Thalamus. *J. Neurosci.* **39,** 692–704 (2019).

38. Usrey, W. M. & Sherman, S. M. Corticofugal circuits: Communication lines from the cortex to the rest of the brain. *J. Comp. Neurol.* **527,** 640–650 (2019).

39. Keshavarzi, S., Bracey, E. F., Faville, R. A., Campagner, D., Tyson, A. L., Lenzi, S. C., Branco, T. & Margrie, T. W. Multisensory coding of angular head velocity in the retrosplenial cortex. *Neuron* **110,** 532-543.e9 (2022).

40. Roth, M. M., Dahmen, J. C., Muir, D. R., Imhof, F., Martini, F. J. & Hofer, S. B. Thalamic nuclei convey diverse contextual information to layer 1 of visual cortex. *Nat. Neurosci.* **19,** 148 (2015).

41. Sullivan, K. E., Kraus, L., Kapustina, M., Wang, L., Stach, T. R., Lemire, A. L., Clements, J. & Cembrowski, M. S. Sharp cell-type-identity changes differentiate the retrosplenial cortex from the neocortex. *Cell Rep.* **42,** 112206 (2023).

42. Zhang, Z., Zhou, J., Tan, P., Pang, Y., Rivkin, A. C., Kirchgessner, M. A., Williams, E., Lee, C.-T., Liu, H., Franklin, A. D., Miyazaki, P. A., Bartlett, A., Aldridge, A. I., Vu, M., Boggeman, L., Fitzpatrick, C., Nery, J. R., Castanon, R. G., Rashid, M., Jacobs, M. W., Ito-Cole, T., O'Connor, C., Pinto-Duartec, A., Dominguez, B., Smith, J. B., Niu, S.-Y., Lee, K.-F., Jin, X., Mukamel, E. A., Behrens, M. M., Ecker, J. R. & Callaway, E. M. Epigenomic diversity of cortical projection neurons in the mouse brain. *Nature* **598,** 167–173 (2021).

43. Rockland, K. S. Distinctive Spatial and Laminar Organization of Single Axons from Lateral Pulvinar in the Macaque. *Vision* **4,** 1 (2019).

44. Rockland, K. S., Andresen, J., Cowie, R. J. & Robinson, D. L. Single axon analysis of pulvinocortical connections to several visual areas in the Macaque. *J. Comp. Neurol.* **406,** 221–250 (1999).

45. Marion, R., Li, K., Purushothaman, G., Jiang, Y. & Casagrande, V. A. Morphological and neurochemical comparisons between pulvinar and V1 projections to V2. *J. Comp. Neurol.* **521,** 813–832 (2013).

46. Grant, E., Hoerder-Suabedissen, A. & Molnár, Z. Development of the Corticothalamic Projections. *Front. Neurosci.* **6,** (2012).

47. Kirchgessner, M. A., Franklin, A. D. & Callaway, E. M. Context-dependent and dynamic functional influence of corticothalamic pathways to first- and higher-order visual thalamus. *Proc. Natl. Acad. Sci.* **117,** 13066–13077 (2020).

48. Crandall, S. R., Cruikshank, S. J. & Connors, B. W. A Corticothalamic Switch: Controlling the Thalamus with Dynamic Synapses. *Neuron* **86,** 768–782 (2015).

49. Cruikshank, S. J., Urabe, H., Nurmikko, A. V. & Connors, B. W. Pathway-Specific Feedforward Circuits between Thalamus and Neocortex Revealed by Selective Optical Stimulation of Axons. *Neuron* **65,** 230–245 (2010).

50. Bourassa, J. & Deschˆnes, M. Corticothalamic projections from the primary visual cortex in rats: a single fiber study using biocytin as an anterograde tracer. *Neuroscience* **66,** 253–263 (1995).

51. Benevento, L. A. & Standage, G. P. The organization of projections of the retinorecipient and nonretinorecipient nuclei of the pretectal complex and layers of the superior colliculus to the lateral pulvinar and medial pulvinar in the macaque monkey. *J. Comp. Neurol.* **217,** 307–336 (1983).

52. Baldwin, M. K. L., Wong, P., Reed, J. L. & Kaas, J. H. Superior colliculus connections with visual thalamus in gray squirrels (Sciurus carolinensis): Evidence for four subdivisions within the pulvinar complex. *J. Comp. Neurol.* **519,** 1071–1094 (2011).

53. Fish, S. E. & Chalupa, L. M. Functional properties of pulvinar-lateral posterior neurons which receive input from the superior colliculus. *Exp. Brain Res.* **36,** (1979).

54. Berman, R. A. & Wurtz, R. H. in *Prog. Brain Res.* **171,** 467–473 (Elsevier, 2008).

55. Bourne, J. A. & Morrone, M. C. Plasticity of Visual Pathways and Function in the Developing Brain: Is the Pulvinar a Crucial Player? *Front. Syst. Neurosci.* **11,** (2017).

56. Homman-Ludiye, J. & Bourne, J. A. The medial pulvinar: function, origin and association with neurodevelopmental disorders. *J. Anat.* **235,** 507–520 (2019).

57. Weiskrantz, L., Warrington, E. K., Sanders, M. D. & Marshall, J. VISUAL CAPACITY IN THE HEMIANOPIC FIELD FOLLOWING A RESTRICTED OCCIPITAL ABLATION.

58. Pöppel, E., Held, R. & Frost, D. Residual Visual Function after Brain Wounds involving the Central Visual Pathways in Man. *Nature* **243,** 295–296 (1973).

59. Sanders, M. D., Warrington, ElizabethK., Marshall, J. & Wieskrantz, L. 'BLINDSIGHT': VISION IN A FIELD DEFECT. *The Lancet* **303,** 707–708 (1974).

60. Bertini, C., Cecere, R. & Làdavas, E. I am blind, but I "see" fear. *Cortex* **49,** 985–993 (2013).

61. Bertini, C., Pietrelli, M., Braghittoni, D. & Làdavas, E. Pulvinar Lesions Disrupt Fear-Related Implicit Visual Processing in Hemianopic Patients. *Front. Psychol.* **9,** 2329 (2018).

62. Takakuwa, N., Isa, K., Onoe, H., Takahashi, J. & Isa, T. Contribution of the Pulvinar and Lateral Geniculate Nucleus to the Control of Visually Guided Saccades in Blindsight Monkeys. *J. Neurosci.* **41,** 1755–1768 (2021).

63. Kinoshita, M., Kato, R., Isa, K., Kobayashi, K., Kobayashi, K., Onoe, H. & Isa, T. Dissecting the circuit for blindsight to reveal the critical role of pulvinar and superior colliculus. *Nat. Commun.* **10,** 135 (2019).

64. Stoerig, P. Blindsight in man and monkey. *Brain* **120,** 535–559 (1997).

65. Ungerleider, L. G. Two cortical visual systems. *Anal. Vis. Behav.* (1982).

66. Mishkin, M. & Ungerleider, L. G. Object vision and spatial vision:two cortical p hways.

67. Goodale, M. A. & Milner, Ad. Separate visual pathways for perception and action. *Trends Neurosci.* **15,** (1992).

68. Kaas, J. H. & Lyon, D. C. Pulvinar contributions to the dorsal and ventral streams of visual processing in primates. *Brain Res. Rev.* **55,** 285–296 (2007).

69. Kaas, J. H. & Baldwin, M. K. L. The Evolution of the Pulvinar Complex in Primates and Its Role in the Dorsal and Ventral Streams of Cortical Processing. *Vision* **4,** 3 (2019).

70. Wang, Q., Gao, E. & Burkhalter, A. Gateways of Ventral and Dorsal Streams in Mouse Visual Cortex. *J. Neurosci.* **31,** 1905–1918 (2011).

71. Gross, C. G. Contribution of striate cortex and the superior colliculus to visual function in area MT, the superior temporal polysensory area and inferior temporal cortex. *Neuropsychologia* **29,** 497–515 (1991).

72. Rodman, H. R., Gross, G. & Albright, D. Afferent Basis of Visual Response Properties in Area MT of the Macaque. I. Effects of Striate Cortex Removal. *J. Neurosci.*

73. Gale, S. D. & Murphy, G. J. Distinct representation and distribution of visual information by specific cell types in mouse superficial superior colliculus. *J. Neurosci. Off. J. Soc. Neurosci.* **34,** 13458–71 (2014).

74. Lavin, T. K., Jin, L. & Wickersham, I. R. Monosynaptic tracing: a step-by-step protocol. *J. Chem. Neuroanat.* **102,** 101661 (2019).

75. Juavinett, A. L., Nauhaus, I., Garrett, M. E., Zhuang, J. & Callaway, E. M. Automated identification of mouse visual areas with intrinsic signal imaging. *Nat. Protoc.* **12,** 32–43 (2017).

76. Wang, Q., Ding, S.-L., Li, Y., Royall, J., Feng, D., Lesnar, P., Graddis, N., Naeemi, M., Facer, B., Ho, A., Dolbeare, T., Blanchard, B., Dee, N., Wakeman, W., Hirokawa, K. E., Szafer, A., Sunkin, S. M., Oh, S. W., Bernard, A., Phillips, J. W., Hawrylycz, M., Koch, C., Zeng, H., Harris, J. A. & Ng, L. The Allen Mouse Brain Common Coordinate Framework: A 3D Reference Atlas. *Cell* **181,** 936-953.e20 (2020).

77. Shamash, P., Carandini, M., Harris, K. & Steinmetz, N. A tool for analyzing electrode tracks from slice histology. *bioRxiv* (2018). doi:10.1101/447995

78. Kim, E. J., Zhang, Z., Huang, L., Ito-Cole, T., Jacobs, M. W., Juavinett, A. L., Senturk, G., Hu, M., Ku, M., Ecker, J. R. & Callaway, E. M. Extraction of Distinct Neuronal Cell Types from within a Genetically Continuous Population. *Neuron* **107,** 274-282.e6 (2020).

79. Zhuang, J., Ng, L., Williams, D., Valley, M., Li, Y., Garrett, M. & Waters, J. An extended retinotopic map of mouse cortex. *eLife* **6,** e18372 (2017).

80. Gilissen, S. R. J., Farrow, K., Bonin, V. & Arckens, L. Reconsidering the Border between the Visual and Posterior Parietal Cortex of Mice. *Cereb. Cortex* **31,** 1675–1692 (2021).

81. Lyamzin, D. & Benucci, A. The mouse posterior parietal cortex: Anatomy and functions. *Neurosci. Res.* **140,** 14–22 (2019).

CHAPTER 2: Investigating the role of the pulvinar in cortical visual function

ABSTRACT

The pulvinar nucleus of the thalamus connects visual cortical areas via parallel, transthalamic relay pathways Many pulvinar projections to extrastriate areas are "core" cells that make strong excitatory connections in the middle cortical layers. Cortical areas therefore have two potential routes for sensory information transfer – direct corticocortical projections and indirect, cortico-pulvino-cortical pathways. While studies in behaving animals have supported a role for the pulvinar in coordinating information transfer between cortical areas, its contribution to overall sensory activity in the cortex is unknown. We investigated the role of the pulvinar in passive extrastriate visual responses using projection-specific inhibitory optogenetics and simultaneous extracellular recordings of the pulvinar and area LM in awake, head-fixed mice. Our results show that the pulvinar only slightly enhances the gain of passive visual responses in the superficial layers of LM, but sensory-evoked activity and feature tuning are preserved in the absence of pulvinar input. This study suggests that direct corticocortical pathways are sufficient for visual information transfer between areas, and that further investigation into the circuit mechanisms of pulvino-cortical interactions likely requires active behavioral contexts to engage the pulvinar.

INTRODUCTION

The expansion of the neocortex over the course of evolution has endowed humans with impressively complex cognitive capabilities. Cortical development, on the scales of both species and individual organisms, is inextricably linked to the commensurate development of the thalamus[1–3]. Thalamocortical interactions serve crucial functions in sleep, cognition, motor control, and sensation[4–7]. The most well-studied thalamocortical pathways are the first-order

(FO) nuclei, which relay peripheral sensory information to the cortex for processing. However, most of the volume of the thalamus is occupied by higher-order (HO) nuclei that connect heavily to higher cortical areas[8,9]. Anatomical evidence suggests that these connections are organized as transthalamic relays between cortical areas[10–12]. HO thalamocortical projections are ubiquitous throughout the cortex, but their role in cortical function is not yet understood.

In the visual system, the pulvinar is a HO thalamic nucleus that has been implicated in spatial attention and visually-guided behavior[13–19]. Pulvinar lesions in humans lead to spatial neglect and deficits in filtering distractors [20–23], and these deficits have been replicated in monkeys with controlled pulvinar lesions[19,24–27]. In cases where cortical activity was also monitored, evidence suggests that pulvinar inactivation reduces the synchrony between and within cortical areas[19]. It is unclear, however, what circuit mechanisms underlie modulation of corticocortical transmission by the pulvinar. Most inactivation studies have assessed pulvino-cortical interactions during various tasks, but it is also possible that the pulvinar input to the cortex supports network activity independent of behavioral context. Pulvinar neurons, while driven strongly by attention or salience, are still responsive to passively presented visual stimuli[15,28,29]. Pulvinar axons arborize in the middle layers of extrastriate cortex, and their driving (Class 1) terminals elicit strong, reliable EPSCs from postsynaptic LM neurons *in vitro* [30–34]. The cortico-pulvino-cortical pathway could therefore drive sensory responses in extrastriate areas, but this possibility has not yet been tested adequately. In the mouse, visual responses in area POR completely depend on superior colliculus activity routed via the pulvinar[35]. Pathways to other extrastriate areas that receive dense pulvinar input from corticorecipient regions, however, have not been tested in a passive condition.

Previous inactivation studies have reported conflicting effects on cortical activity[19,36–39] (See Appendix Table 2.S1 for review), and technical limitations make interpreting the results difficult. The pulvinar sends distinct projections to a large number of cortical targets, and the somata of these projections are spatially intermixed[10,40,41]. Any nonspecific inactivation method thus affects the thalamocortical inputs to many cortical areas, which could cause off-target effects. Furthermore, optogenetic hyperpolarization with chloride or hydrogen pumps is ineffective at silencing thalamic activity, instead shifting the firing of neurons into burst mode[42]. With the recent development of highly efficient chloride channels, however, powerful and precise inactivation of thalamic neurons is now feasible[43].

To assess the role of the pulvinar in cortical sensory processing, we used a retrograde targeting strategy to drive cre-dependent expression of the inhibitory opsin, stGtACR2, in pulvinar neurons projecting to the lateromedial (LM) visual area, a homolog to primate area V2[44]. We effectively silenced thalamic activity while simultaneously recording extracellular activity in the thalamus and cortex. Thalamocortical transmission in the FO circuit was blocked, confirming our optogenetic efficacy. Inactivation of the HO circuit, however, resulted in only modest suppression of visual activity in the superficial layers of LM. Most single units were unaffected by the optogenetic manipulation. Despite the slight, layer-specific reduction in response magnitudes, tuning for stimulus orientation was unaffected. This study resolves previous uncertainty due to imprecise thalamic inactivation, and shows that the pulvinar is not necessary for sensory responses in extrastriate cortex. Applying this targeted inactivation approach in combination with spatial attention tasks could finally reveal the mechanisms by which the pulvinar controls cortical communication.

RESULTS

Targeted inactivation of Pulvinar→LM projection neurons

The pulvinar sends extensive excitatory projections to extrastriate cortex, but the role of this pathway in sensory processing is unknown. To inactivate pulvinar projections to a single higher visual area (HVA) in the mouse during passive visual stimulation, we used a retrograde targeting strategy to drive cre-dependent expression of a light-activated chloride channel, stGtACR2, in LM-projecting pulvinar neurons. By optogenetically inactivating pulvinar projections while simultaneously recording extracellular activity from the cortex and thalamus (Fig 2.1), we assessed the contribution of the pulvinar to LM visual activity.

We used intrinsic signal imaging to target injections of AAV5-Cre, which is effectively retrogradely transported along long-range thalamocortical axons, into LM. Cre-dependent stGtACR2 in the pulvinar was reliably expressed throughout the subdivisions of the pulvinar, following the spatial distribution of LM projection neurons that has been previously reported with other retrograde tracers[40,41]. A subset of injections in the cre-reporter mouse Sun1/sfGFP verified that opsin was efficiently expressed in almost all cre^+ projection neurons (Fig 2.1D).

Projection-specific stGtACR2 inactivation abolishes visual responses in the first order thalamocortical pathway

Optogenetic inactivation of thalamic neurons has remained a technical challenge due to hyperpolarization-activated currents and persistent oscillatory activity between relay cells and the thalamic reticular nucleus (TRN). Previous attempts to inactivate the dLGN and pulvinar (unpublished, this author) or the primary somatosensory thalamus, VPM[45], with the light-activated chloride pump, halorhodopsin, have instead shifted cells into burst firing mode, which preserves sensory evoked activity[42,46]. Since stGtACR2 provides much higher photocurrents

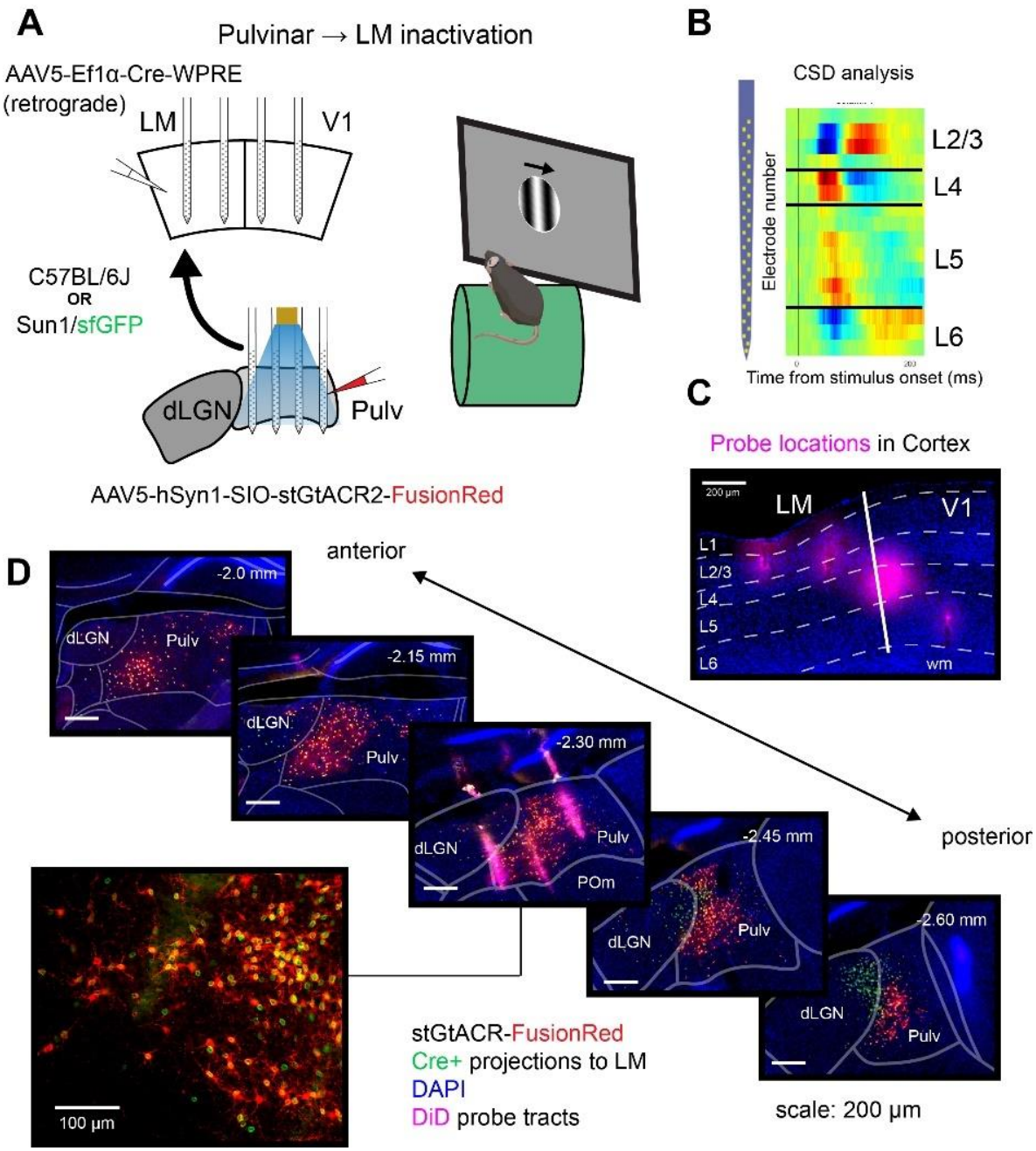

Figure 2.1 Inactivating pulvinar projections to area LM during visual stimulation.A) Schematic of experiment. Pulvinar projections to LM are targeted with an AAV expressing cre-dependent stGtACR2 and a retrograde AAV-Cre in LM. Extracellular recordings from cortex and the pulvinar were acquired from awake, headfixed mice during presentation of drifting sinusoidal gratings. **B)** Current source density analysis (CSD) defines the laminar location of electrodes across the shanks in cortex. Scale bar = 200 µm. **C)** Post-mortem histological verification of probe locations. D) top series: Post mortem histological verification of opsin expression and probe locations in the pulvinar along the rostro-caudal extent of the pulvinar. Scale bars = 200 µm. Bottom-right: higher magnification of cells in image 3 showing coexpression of GFP and stGtACR2-FusionRed in a Sun1-sfGFP cre reporter mouse. Scale bar = 100 µm.

and additional shunting inhibition[43], we tested its efficacy in dLGN→V1 projections, which are necessary for sensory-evoked activity in V1. Using the same viral targeting strategy, we expressed cre-dependent stGtACR2 in a restricted subset of dLGN neurons that projected to the posterior, lateral portion of V1 (Fig 2.2A-B).

We inactivated the dLGN→V1 pathway in awake, headfixed mice, and effectively abolished V1 responses to small drifting grating stimuli (Fig 2.2C-G) . Optogenetic inactivation completely suppressed dLGN neurons throughout the duration of LED stimulation (Fig2.2C). Suppression was spatially restricted in the dLGN to the region of opsin expression (Fig 2.2B,D). Both visually evoked and spontaneous activity in V1 was similarly suppressed for the duration of LED stimulation (Fig 2.2E). Suppression was consistent across the population of recorded units (37/44 units (84%), $p_{adj}<0.05$, Wilcoxon rank-sum test with Benjamini-Hochberg correction for false discovery rate) with more complete suppression observed in granular and supragranular layers (Fig 2.2 F,G).

The pulvinar provides modest enhancement of LM responses, but does not drive visual responses or selectivity

After validating our inactivation method in the first-order thalamocortical pathway, we evaluated the effects of inactivating Pulvinar→LM projections. Unlike the dLGN, where projections to a given region of V1 are tightly clustered, LM-projecting neurons are distributed throughout the pulvinar nucleus and are interspersed with neurons projecting to other cortical areas[41]. By design, these neurons did not express the opsin, so the majority of recorded pulvinar units we recorded were not inactivated (Fig 2.3B). However, units that were inactivated were totally suppressed by optogenetic stimulation for the entire duration of the LED pulse (Fig 2.3A). Despite not sampling many inactivated pulvinar units, the whole population of stGtACR2-

Figure 2.2 Thalamocortical inactivation eliminates visual responses in V1. A) Schematic of dLGN control experiment. Focal injection of AAV-Cre in V1 retrogradely infects thalamic axons to activate cre-dependent stGtACR2. After expression, multishank probes in V1 record in vivo responses to drifting gratings while an optrode in dLGN delivers blue light for optogenetic inhibition. **B)** Locations of optical fiber (large arrow) and probe shanks (small arrows) are marked with DiD (magenta) and confirmed with post-mortem histology. Targeted projection neurons express stGtACR2 (red). Cre+ cells express GFP (green). Scale bars = 300 μm. **C)** Example inactivated dLGN unit. Top left: Peri-stimulus time histogram for all trials with visual stimulation. Black trace: LED off trials; Blue trace: LED on trials. The gray box highlights the visual stimulation period. The blue line marks the period of LED stimulation, beginning 50 ms prior to visual stimulus onset until 50 ms following visual stimulus offset. Top right: Same as top left for blank trials (no visual stimulus). Bottom left: Spike raster for LED off (black) and LED on (blue) visual trials. The gray box indicates the visual stimulation period. Bottom right: Same as bottom left for blank trials. **D)** dLGN population activity. Top: Light modulation index (LMI) by depth. Negative LMI values correspond to suppressed units, and positive values correspond to activated units. A depth of zero is defined as the deepest electrode contact in dLGN. N = 90 units from 1 animal. Units with significantly light-modulated firing rates are shown with filled circles ($p_{adj}<0.05$, Wilcoxon rank-sum test with Benjamini-Hochberg correction for false discovery rate). Open circles show units with non-significant light modulation. Units in red are between 300-500 μm depth, defined as the putatively infected zone of dLGN. Units in black are outside of this range. Bottom: Average firing rates during the visual stimulation period for LED on trials versus LED off trials. Markers denote significant modulation and depth as in top panel. Linear regression (red line) fit to suppressed units in the putatively infected zone. **E)** Same as (C), but for a V1 unit from a different animal. Onset of LED 200 ms prior to visual stimulus onset. Offset of LED 100 ms following visual stimulus offset. **F)** Same as (D), but for a population of 44 units in a separate animal. **G)** Multiunit activity (Hz) in V1, separated by cortical layer. LED off (black) average MUA compared to LED on (blue) average MUA. Gray box indicates visual stimulation period. Blue line shows period of LED stimulation.

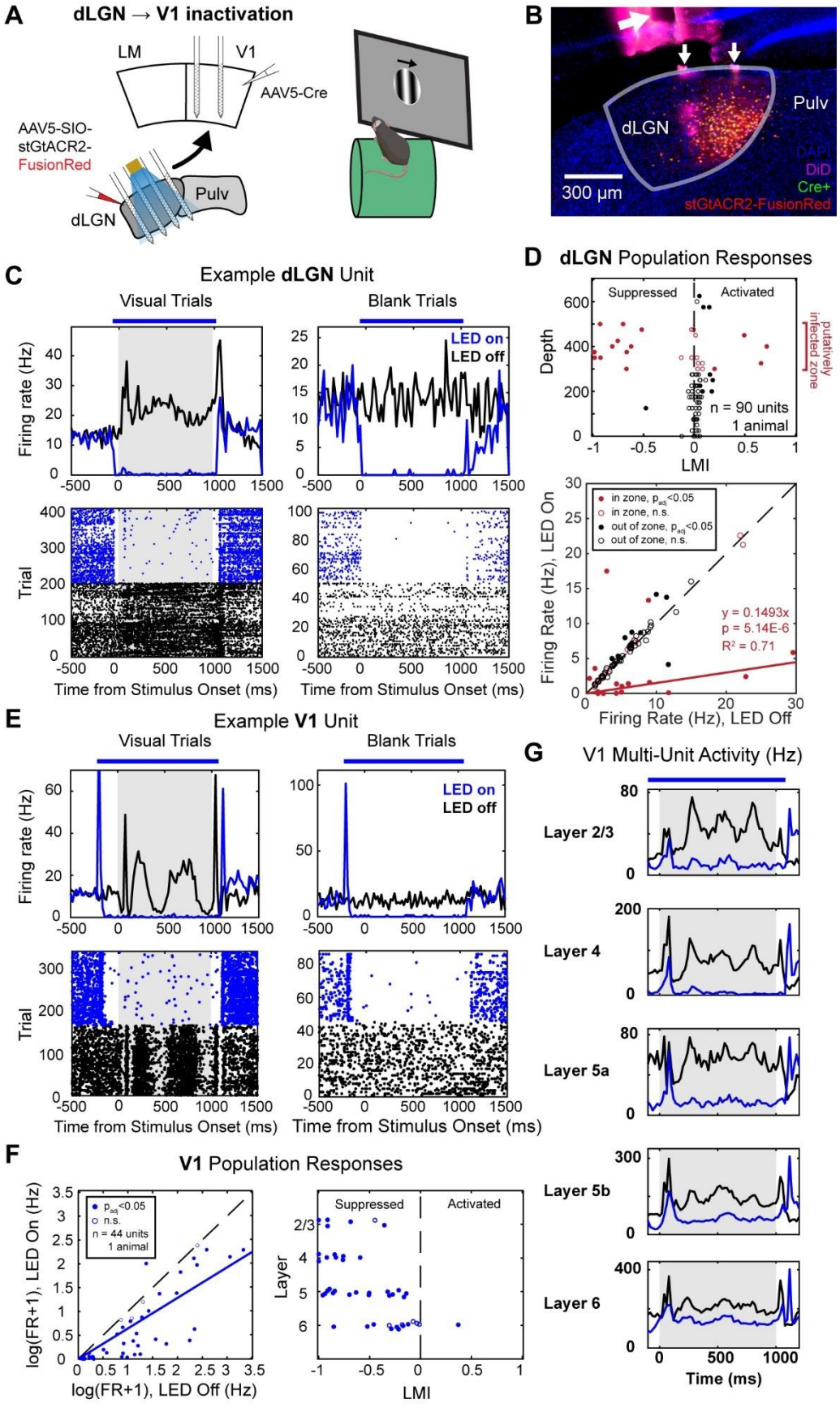
A
dLGN → V1 inactivation
LM
V1
AAV5-Cre
AAV5-SIO-stGtACR2-FusionRed
Pulv
dLGN
B
Pulv
dLGN
DAPI
DiD
Cre+
stGtACR2-FusionRed
300 µm
C
Example dLGN Unit
Visual Trials
Blank Trials
LED on
LED off
Firing rate (Hz)
Trial
Time from Stimulus Onset (ms)
D
dLGN Population Responses
Suppressed
Activated
Depth
putatively infected zone
n = 90 units
1 animal
LMI
in zone, p_adj<0.05
in zone, n.s.
out of zone, p_adj<0.05
out of zone, n.s.
y = 0.1493x
p = 5.14E-6
R² = 0.71
Firing Rate (Hz), LED On
Firing Rate (Hz), LED Off
E
Example V1 Unit
Visual Trials
Blank Trials
LED on
LED off
Firing rate (Hz)
Trial
Time from Stimulus Onset (ms)
F
V1 Population Responses
p_adj<0.05
n.s.
n = 44 units
1 animal
log(FR+1), LED On (Hz)
log(FR+1), LED Off (Hz)
Suppressed
Activated
Layer
LMI
G
V1 Multi-Unit Activity (Hz)
Layer 2/3
Layer 4
Layer 5a
Layer 5b
Layer 6
Time (ms)

pulvinar in every experiment. Additionally, we used a light power density of ~5 mW/mm^2, which we estimated to be effective at least 1 mm away from the fiber tip based on modeled light scattering in tissue and reported inactivation efficacy[43,47]. Of the visually responsive units isolated in LM (155/221 (70%) units, n = 7 mice, See Methods), 41 (26%) were significantly significantly modulated by pulvinar inactivation (Wilcoxon rank-sum test with Benjamini-Hochberg correction). However, the magnitude of observed effects was small (Fig 2.3C,D; LMI for suppressed units: -0.18±0.02 mean±SEM, n = 27/155 units; LMI for activated units: 0.13±0.02 mean±SEM, n = 14/155 units). Some units were not modulated by pulvinar inactivation for *all* visual trials, but still showed some reduction in firing at their preferred stimuli (Fig 2.3 C,D). Overall, the orientation selectivity for the population of LM units was not significantly different for LED on and LED off trials (ΔOSI = -0.1571±0.1017 mean±SEM, p_{adj} = 0.1591, Wilcoxon sign-rank test with Benjamini-Hochberg correction).

Pulvinar projections to LM primarily target layer 2/3 and upper layer 4. We typically recorded fewer well-isolated single units from layer 2/3 due to smaller spike amplitudes and sparser firing than deeper layers. To assess the population effects of pulvinar inactivation with a method that was robust to these spike-sorting biases, we compared multi-unit activity (MUA) in each layer of one example animal for LED on and LED off trials. Consistent with a modest excitatory pathway, optogenetic inactivation of the pulvinar slightly, but significantly, reduced MUA in upper cortical layers and in layer 5B ($LMI_{L2/3}$ = -0.1019, p = $1.07x10^{-9}$; LMI_{L4} = -0.0792, p = 1.87x10-^{16}; LMI_{L5A} = -0.0159, p = 0.10 (n.s.); LMI_{L5B} = -0.0434, p = $8.52x10^{-8}$; LMI_{L6} = 0.0104, p = 0.74 (n.s.); Wilcoxon rank-sum test with 0.01 significance level). Layer 5A and layer 6 MUA was unaffected by pulvinar inactivation. Pulvinar inactivation had no effect on

Figure 2.3 LM visual responses do not depend on pulvinar activity. A) Left: Multi-shank recordings in the pulvinar. Center & Right: Peri-stimulus time histogram for two example inactivated pulvinar units. Black – mean firing rate (Hz) during LED off visual trials. Blue – mean firing rate (Hz) during LED on visual trials. Shaded gray area indicates the epoch where drifting grating stimuli are presented. Horizontal blue line marks the period of LED stimulation for LED on trials, which was 50 ms prior to visual stimulus onset until 50 ms after visual stimulus offset. **B)** Scatter plot of firing rates (Hz) during 1 s visual stimulation epoch for LED on trials vs LED off trials for all well-isolated single pulvinar units (n=184) from 5 animals. Filled circles indicate significantly modulated firing ($p_{adj}<0.05$, Wilxocon rank sum test with Benjamini-Hochberg correction for false discovery rate). Open circles indicate non-significant firing rate modulation. **C)** Three example LM units. Top row: Peri-stimulus time histogram, as in (A). Center row: Spike raster plots for LED off (black) and LED on (blue) trials. Shaded gray area indicates the epoch where drifting grating stimuli are presented. Horizontal blue line marks the period of LED stimulation for LED on trials. Bottom row: Orientation tuning curves. Mean firing rates (Hz) at each orientation (degrees) for LED off (black) and LED on (blue) trials. When temporal frequency (tf) or spatial frequency (tf) were also varied, means were taken at the preferred tf and sf. Error bars indicate standard error of the mean (SEM). **D)** Population responses in LM (n = 155 units from 7 animals). Top left: Scatter plot of firing rates for all visual trials, as in (B). Bottom left: Scatter plot of firing rates for preferred stimuli only for the same units in top left. Top right: Light modulation index (LMI) for LM units by cortical layer. Filled circles indicate significantly modulated firing rates ($p_{adj}<0.05$, Wilxocon rank sum test with Benjamini-Hochberg correction for false discovery rate). Open circles indicate non-significant firing rate modulation. Bottom right: Histogram of orientation selectivity index (OSI) difference between light on and light off trials. OSI is defined as the difference between mean firing rates at the preferred stimulus and the average of two orthogonal stimuli over their sum. Mean ΔOSI = -0.1571, p = 0.1591 (Wilcoxon signed rank test). **E)** Multi-unit activity (MUA) in LM separated by cortical layer for one example animal. Peristimulus time histogram of mean MUA (Hz) for LED off (black) trials and LED on (blue) trials. Shaded gray area indicates the epoch where drifting grating stimuli are presented. Horizontal blue line marks the period of LED stimulation for LED on trials.

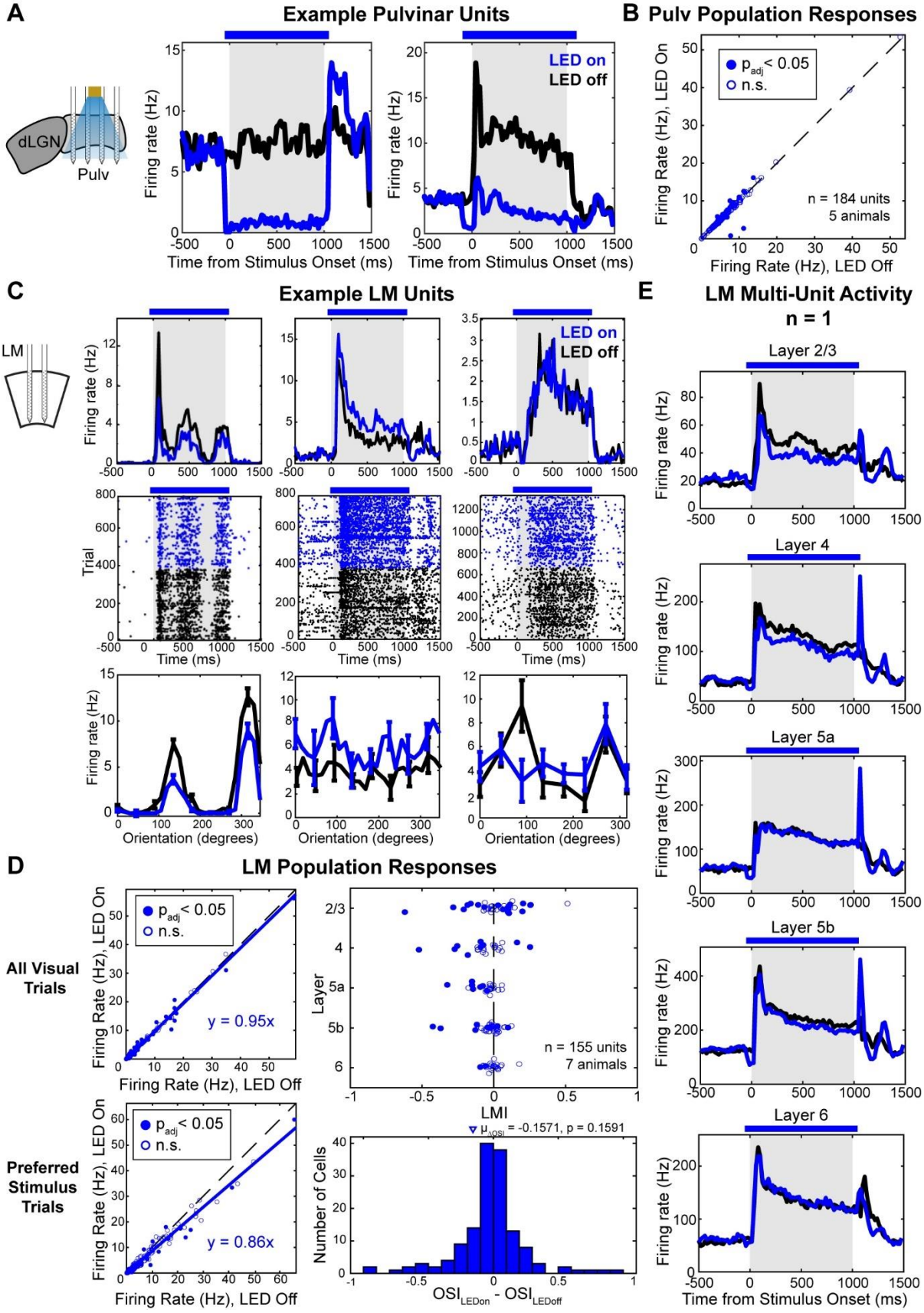
A
Example Pulvinar Units
dLGN
Pulv
Firing rate (Hz)
LED on
LED off
Time from Stimulus Onset (ms)
B Pulv Population Responses
p_{adj} < 0.05
n.s.
Firing Rate (Hz), LED On
Firing Rate (Hz), LED Off
n = 184 units
5 animals
C
Example LM Units
LM
Trial
Time (ms)
Orientation (degrees)
D
LM Population Responses
All Visual Trials
Preferred Stimulus Trials
y = 0.95x
y = 0.86x
Layer
2/3
4
5a
5b
6
n = 155 units
7 animals
LMI
μ_{OSI} = -0.1571, p = 0.1591
Number of Cells
OSI_{LEDon} - OSI_{LEDoff}
E
LM Multi-Unit Activity
n = 1
Layer 2/3
Layer 4
Layer 5a
Layer 5b
Layer 6
Time from Stimulus Onset (ms)

spontaneous MUA during blank trials, except for in layer 5b, where MUA was significantly suppressed ($LMI_{L2/3}$ = -0.0654, p = 0.31 (n.s.); LMI_{L4} = -0.0718, p = 0.14 (n.s.); LMI_{L5A} = 0.0476, p = 0.20 (n.s.); LMI_{L5B} = -0.1240, p = $5.55x10^{-5}$; LMI_{L6} = -0.0476, p = 0.68 (n.s.); Wilcoxon rank-sum test with 0.01 significance level). Interestingly, suppression of L5b spontaneous activity was slightly greater than suppression of visually-evoked activity (ΔMUA_{visual} = -21.87±18.22 Hz (Mean±SEM), $\Delta MUA_{spontaneous}$ = -32.07±19.85 Hz (Mean±SEM)).

Despite some significant differences in LM population responses with pulvinar inactivation, we found only modest effect sizes. Overall, the tuning properties and visual responses of LM neurons were not drastically different when pulvinar input was removed. Because identical optogenetic manipulation of the primary visual thalamocortical pathway produced profound deficits in cortical sensory responses, these small effects demonstrate a minimal role for the pulvinar in passive visual processing rather than incomplete or inadequate inactivation of the pulvinar.

DISCUSSION

As demonstrated in Chapter 1, transthalamic pathways between cortical areas mirror the direct corticocortical pathways in the visual hierarchy. This provides a potentially redundant circuit for the transfer of sensory information. Our anatomical results suggest that the pulvinar relays a signal from V1 to LM across two "driving" synapses. To determine whether this relay plays a meaningful role in sensory transmission *in vivo*, we optogenetically inactivated the pulvinar→LM projection in awake, headfixed mice during the presentation of visual stimuli. Contrary to the anatomical implication, we found that visually evoked activity and orientation selectivity in LM were largely preserved. We observed modest suppression of a minority of

single units and MUA in LM that was specific to cortical layers. MUA was reduced primarily in layer 2/3 and layer 4, which is the region innervated by "core" type pulvinocortical terminals[33]. This suppression did not propagate to the entire column, as layer 5a and layer 6 were unaffected.

One difficulty with interpreting small downstream effects from inactivation experiments is potential uncertainty about the effectiveness of the directly inactivating a population of cells. We simultaneously recorded the activity of pulvinar neurons during the inactivation, and saw a handful of fully suppressed cells. Since projections to LM are spatially intermingled with projections to other visual areas that were not injected with AAV-Cre this is probably due to limited sampling with the linear probes. Optogenetic suppression with a step pulse usually evoked rebound spiking in our experiments. MUA in LM shows strong rebound responses for LED on trials at the light offset, providing additional confirmation that our manipulation was having widespread network effects in the thalamus. Modulated cells were either very slightly modulated by optogenetic stimulation, or they were completely suppressed. Additionally, increasing light power did not provide additional suppression of either pulvinar or cortical units. This bimodal suppression suggests that individual cells are being effectively and maximally suppressed, but it leaves open the possibility that only a subset of the pulvinar→LM projection neurons are expressing the opsin. Because the expression of stGtACR covered a large extent of all pulvinar subdivisions and was almost entirely coexpressed with a cre-reporter marker, it is unlikely that the AAV-stGtACR2 viral efficiency could explain the small effects observed. Without a positive control, we could not rule out AAV5-Cre inefficiency as a contributing factor. Therefore, we repeated the same viral and optogenetic parameters in the FO thalamocortical nuleus, where V1 visual responses are known to depend on dLGN activity. Inactivating a small

subset of dLGN neurons with identical methods caused a profound reduction in V1 visual responses, confirming the overall efficacy of our inactivation strategy.

By ruling out technical explanations for a modest optogenetic effect, we conclude that the pulvinar pathway to LM does not drive visual responses in cortex. The transthalamic pathway is therefore not an exactly redundant pathway to the corticocortical projection from V1 to LM. Our findings support previous theoretical estimates of projection numbers and receptive field sizes that cast doubt on the hypothesis that transthalamic relays would drive sensory activity[48]. Due to the many differences in species, inactivation method, brain areas, and behavioral state used in previous inactivation studies (Appendix Fig 2.S1), it is difficult to make direct comparisons between our results and other studies. Pharmacological and optogenetic inactivation of the SC, which projects to cortex indirectly through the pulvinar, completely abolished responses in area POR[35]. This is likely due to differential circuit wiring of pulvinar→LM from pulvinar→POR projections. POR gets extensive projections from the caudal pulvinar, which receives dense input from the SC, but not V1[49]. Its motion sensitivity and strong disynaptic SCs input could justify a comparison to area MT in the dorsal stream of primates[50]. LM, however, is more similar to V2 in that it receives a very strong input from V1 and its border with V1 reflects a retinotopic reversal about the vertical meridian[44]. Since LM receives strong direct corticocortical input as well as pulvinar input from both cortico- and tecto-recipient zones, it is an adequate model to test the differences between these pathways. Additional experiments blocking terminal release from V1 projections in combination with pulvinar inactivation would help to compare these pathways more directly.

Our results align with those reported in Zhou et al., 2016 (change detection task) and Eradath et al., 2021 (passive viewing), with some important distinctions[19,37]. Zhou et al. observed

increased spontaneous firing rates, and a broad decrease in evoked rates in response to a visual stimulus. We did not observe significant changes in baseline firing, except for in L5b, where it was suppressed. Additionally, we only observed reduced evoked responses in a minority of cells. Muscimol inactivation occurs over a longer time course than optogenetic inactivation, so there could be homeostatic compensation somewhere in the network that might change baseline firing. Additionally, muscimol inactivation is non-specific, so pulvinar neurons to multiple areas would have been inactivated. Perhaps the most relevant distinction between Zhou et al. and Eradath et al., which did not find significant changes in firing rates, is the stimulus and task context. While the cue that evoked initial responses was not presented in the period where attentional modulation would have been occurring, monkeys were still engaged and paying attention to the screen. In our study and in Eradath et al., animals were not engaged in a task. Therefore, pulvinar effects on cortical responses may not be relevant in the context of passive viewing. We did observe some reduced responses, however, which were not observed in Eradath et al. This difference could be due to the stimuli used. In that study, monkeys viewed a movie with natural scenes, which are known to cause lower evoked firing than small, low dimensional, high contrast gratings. If pulvinar modulates cortical activity in a multiplicative manner, then, it might be even less relevant for passive viewing of natural stimuli.

Some reports of pulvinar responses find fewer than half of cells to be visually responsive[28], and many neurons instead or in conjunction reflect eye movements, motion mismatch, perceptual awareness, auditory, somatosensory, nociceptive, and other features[15,16,18,51–55]. Given the diverse features which are represented in the pulvinar, perhaps, like perception itself, we will not be able to understand its function with overly reductive methods.

METHODS

Animals

Five adult female and male C57BL/6J mice (The Jackson Laboratories) and four R26R-CAG-loxp-stop-loxp-Sun1-sfGFP-Myc (INTACT) mice maintained on a C57BL/6J background were included in this study. All animals were between 6-10 weeks of age at the time of procedures. All experimental procedures followed procedures approved by the Salk Institute Animal Care and Use Committee.

Viruses

AAV5-Ef1α-Cre-WPRE (UNC Vector Core)

AAV1-hSyn1-SIO-stGtACR2-FusionRed (~$1x10^{12}$ GC/mL; Addgene)

AAV5-hSyn1-SIO-stGtACR2-FusionRed (~$1x10^{12}$ GC/mL; Vigene Biosciences)

Surgical Procedures

For thalamic injections, mice were anesthetized with isoflurane (2% induction; 1.5% maintenance) and mounted in a stereotax (David Kopf Instruments Model 940 series). A small craniotomy was drilled over the left hemisphere to access the thalamus. Coordinates used for pulvinar injections were -1.95 mm posterior to bregma, -1.45 mm relative to the midline. dLGN injections were made at -2.20 mm posterior to bregma, -2.00 mm relative to the midline. A glass pipette loaded with the AAV-stGtACR2 virus was slowly lowered 2.6 mm below the pia. 150 nL of virus was pressure injected with a syringe at a rate of 10 nL/min. The pipette was then raised for a second injection of 150 nL at 2.4 mm below the pia. After the second injection, the pipette was retracted to -2.35 mm and left in place for 10 minutes before retracting completely. For injections targeting dLGN→V1 projections, a second injection of AAV-Cre was made into V1 at 0.50 mm anterior to the lambda suture and -2.6 - -2.8 relative to the midline. Virus was injected

at 500 µm (40 nL) and 300 µm (35 nL) below the pia. The pipette was left in place for 1 minute before retracting and closing the incision with Vetbond (3M). For injections targeting pulvinar→LM projections, a circular metal headframe was attached to the skull with dental cement (C&B Metabond, Parkell) during the same surgery to prepare for subsequent intrinsic signal imaging. For dLGN→V1 experiments, a headframe was attached one week prior to recording, and the skull was covered with Kwik-kast. Mice received either a subcutaneous injection of Meloxicam (5 mg/kg) or buprenex SR (0.5-1.0 mg/kg) for post-operative analgesia. If buprenex was administered, mice also received ibuprofen in their home cage water bottle.

To target LM for viral injections, we mapped the HVAs using intrinsic signal imaging (see below) 1-4 days after the headframe placement. After imaging, mice were anesthetized with isofluorane (1.5%) and secured to a headframe holder. The blood vessel map was used to determine the placement of a small craniotomy over the center of LM. A glass pipette loaded with AAV-Cre virus was lowered to 500 µm below the pia for an initial 40 nL injection. A second injection of 35 nL was made at a depth of 300 µm. After leaving the pipette in place for 1-5 minutes, the pipette was retracted, and the skull was covered with a silicone elastomer (Kwik-kast, World Precision Instruments). Mice that previously received meloxicam were given a dose of buprenex SR (0.5-1.0 mg/kg) subcutaneously and ibuprofen in a water bottle. Mice that previously received buprenex were given an additional dose 3 days after the first dose. Mice recovered in their home cages for 2 weeks before being gradually habituated to a cylindrical treadmill.

Intrinsic Signal Imaging

The borders of LM were identified using intrinsic signal imaging (ISI) as previously described[56,57]. Mice were anesthetized with 0.1-1% isoflurane and sedated with (1 mg/kg)

chlorprothixene hydrochloride injected intramuscularly. To prevent infection of the skull over the 3 week recovery period, the skull was thinned with a carbide burr as little as possible. During presentation of a drifting checkerboard stimulus to the right eye, anesthesia was continuously monitored and adjusted to maintain a lightly anesthetized state (1-1.5 breaths/second). The resulting map of visual cortex was used to guide cortical injections and to target silicon probes to LM and/or V1.

***In vivo* electrophysiology**

Prior to recording, mice were gradually habituated to head fixation on a cylindrical treadmill for 4-7 days, starting with 15 minute sessions and building up to one hour/day. On the day of recording, mice were anesthetized with 1.5% isofluorane. Two large craniotomies were made over the cortical and thalamic recording sites. Until the electrode penetrations were made, the cortical surface was flooded with ACSF to prevent tissue drying. Mice were then headfixed above a treadmill, where they recovered from anesthesia. Treadmill movement was tracked with a rotary encoder.

Once mice were awake and active, a 128-channel silicon microprobe[58,59] (128D) was lowered into the thalamus with a digital manipulator (Sutter Instrument, MP-285), slightly lateral and posterior to the pulvinar injection site to account for headframe angle. This probe was used to map the activity in the thalamus and to determine the location of the pulvinar based on firing properties and visual responsiveness. Our targeting strategy was to locate the dLGN based on its high spontaneous firing, high proportion of visually responsive cells, and linear visual responses to drifting sinusoidal gratings. Shanks medial to the dLGN were likely in the pulvinar, and typically had lower spontaneous and evoked firing rates with mixed visual responsiveness. This mapping procedure typically took less than 3 penetrations. When the pulvinar was found, we

switched the 128-channel probe with a custom 128-channel optrode (Fig 2.1A; 128DN geometry), which had an attached 200 µm diameter core, 0.22 NA optical fiber (ThorLabs, FG200UEP) placed between the 2nd and 3rd shanks such that the tip was immediately above the top contacts of the electrodes.

Cortical and thalamic probes were coated with DiD (2.5% in DI water, Thermo Fisher, D7757) to verify recording locations with post-mortem histology. The optrode was positioned at the previously mapped location and slowly lowered ~1 mm. It was not lowered to the final position until the cortical probe was placed. For cortical recordings, the ISI map guided placement of either a 2 shank 128-channel probe (128AN) in the injected area of LM or a 4 shank 128-channel probe (128D) across the border of V1 and LM such that 2 shanks were in each area, oriented along the azimuth gradient for approximately matched retinotopy. The headframe chamber was flooded with 3% agar (Sigma-Aldrich, A9793 in ACSF) to stabilize the brain and probes. The cortical probe was slowly lowered with a manual manipulator (David Kopf Instruments) until the top electrode contact was in the brain. A The optrode was lowered until only the top few contacts on each shank were in the hippocampus, determined by visual inspection of online LFP theta oscillations and reduced spiking. ACSF was poured over the agar and maintained throughout the recording to prevent drying. Before beginning a recording, probes rested in place for at least 30 minutes. Each probe was connected to a 128-channel headstage (Intan Technologies, C3316) for signal amplification and digitization. Signals were sampled at 25 kHz with an OpenEphys data acquisition system[60].

Optogenetic stimulation

The proximal end of the optrode fiber was attached to a ferrule and connected to a 470 nm LED (Thorlabs, M470F4 with T-cube driver LEDD1B**)** coupled to a 200 µm diameter core,

0.22 NA patch cable (ThorLabs). Prior to optrode fabrication, light power through each fiber was calibrated with a power meter (ThorLabs; PM100D with 1.S121C power sensor). An Arduino Zero board controlled the LED driver to deliver step pulses of light. The current output was set for each new optrode to a level that would result in ~5 mW/mm^2 irradiance at the fiber tip. In control experiments, varying the light power from 1-20 mW/mm^2 did not result in additional suppression of either pulvinar or cortical activity beyond 5 mm/mW^2. Half of all trials were pseudorandomly assigned to be LED on trials. The light pulse began 50 ms before the visual stimulus onset and ended 50 ms after the visual stimulus offset. On a subset of dLGN inactivation experiments, this timing was varied to 200 ms before visual stimulus onset and a coincident offset with the visual stimulus.

Visual Stimulation

Visual stimuli were generated using the Psychtoolbox Matlab package and displayed on a 24" LED monitor (GL2450-B, BenQ) with 60 Hz refresh rate. The screen was positioned 12 cm away from the left eye of the mouse at a nasal-temporal angle of approximately 20°. All stimuli were presented at full contrast. A photodiode attached to the monitor recorded the stimulus output for accurate syncing of neural responses. After placing the microelectrodes and prior to beginning a recording, a small, 5-20° circular drifting grating stimulus was moved around the monitor to locate the approximate center of the recorded units' receptive fields. An audio monitor played the spiking activity, and the azimuth position with maximum evoked spiking during visual stimulation was selected as the center for subsequent stimuli. When receptive fields were noticeably offset between shanks, the center was selected between the two preferred locations in order to drive activity on both shanks.

For pulvinar recordings, 50° circular drifting sine wave gratings were presented, which

were vertically centered and extended across the height of the monitor. The spatial frequency of gratings was 0.04 cycles per degree, and temporal frequency was 2 Hz. Stimuli were pseudorandomly presented at 4-12 orientations, with 2 directions per orientation. A subset of experiments also varied in spatial frequency from 0.02-0.08 cycles per degree and/or 1-4 Hz temporal frequency. Trials were 2 seconds long. Visual stimuli appeared 500 ms after the start of a trial and lasted for 1 second. Intertrial intervals ranged from 1-2 seconds. An equiluminent gray screen was displayed before and after the visual stimulus. To analyze spontaneous firing rates, 20% of trials were "blank", with only a gray screen displayed. Total number of trials varied from 1000-2400 (~1-2 hours) to give at least 16 repeat presentations of each unique stimulus.

For dLGN inactivation experiments, stimuli were 5-20°, and centered on the preferred azimuth and elevation determined from manual receptive field mapping. Stimuli were presented at 0.02 cycles per degree at 1 Hz temporal frequency, with all other parameters equal to those described above for pulvinar recordings.

During the initial placement of cortical probes and after the conclusion of each experiment, we ran a 2 minute long, full field, flashed stimulus for current source density (CSD) analysis. The screen alternated between light and dark on a 50% duty cycle with 4 second period.

Histology

Immediately after a recording ended, mice were euthanized with an intraperitoneal injection of Euthasol (15.6mg/ml), then transcardially perfused with phosphate-buffered saline (PBS) followed by 4% paraformaldehyde (PFA). After dissection, brains were post-fixed in 2% PFA and 15% sucrose in PBS for 16-24 hours at 4°C, then submerged in 30% sucrose for an additional 16-24 hours at 4°C.

We made 50 μm thick, coronal sections of brains using a freezing microtome for post-

mortem identification of electrode tracks and confirmation of opsin expression. Sun1/sfGFP brains underwent immunohistochemical staining to amplify the nuclear GFP signal. After blocking the free-floating sections in PBS with 5% NDS and 1% Triton-X for 1 hour at room temperature, we incubated the tissue with goat anti-GFP (1:500; 600-101-215; Rockland Immunochemical) in PBS with 1% NDS and 0.5% Triton-X for 16-24 hours at 4°C. The tissue was then incubated for 2 hours at room temperature with donkey anti-goat conjugated to Alexa Fluor 488 (1:500; A-11055; Thermo-Fisher), then counterstained with DAPI. Wild-type brains were stained with DAPI only. We mounted tissue on glass slides and coverslipped them with polyvinyl alcohol mounting medium containing 1,4-diazabicyclo-octane (PVA-DABCO).

Slides were scanned using cellSens on an Olympus BX63 microscope with 10X objective. A subset of Sun1/sfGFP thalamic sections were scanned with a 20X objective at 5 µm focal plane increments.

Quantification and Analysis

Single Unit Isolation

We used Matlab to remove light artifacts from the raw data before spike sorting, which allowed us to detect true spikes that occurred within a couple milliseconds of the light artifacts. LED onset and offset timestamps were derived from the analog input signal to the LED driver. For each channel, we calculated the average signal in a window equal to the duration of LED stimulation, starting 2 ms prior to LED onset for all LED on trials. We repeated this calculation for the average signal triggered by the LED offset. The resulting artifacts were then subtracted from the raw signal, which was saved as a new binary file.

We used Kilosort v2.5[61,62] to automatically detect and cluster spike waveforms into putative single units. The corrected voltage signals were band-pass filtered with cutoffs of 300

and 5000 Hz. Clusters were manually inspected using Phy[63] for refractory period violations, oversplitting, and artifacts/noise. Clusters with clear spiking waveforms but poor isolation were classified as multi-unit activity (MUA). Well-isolated clusters were included for analysis if they met several additional quality metrics. We excluded units with an estimated false positive rate greater than 0.1 or a mahalanobis distance less than 15[64,65]. We also inspected the firing rates of each unit over the duration of the recording. If units "dropped out," and did not maintain firing throughout the recording, we limited analysis to the trials during which the unit was present.

Classification of thalamic units

To confirm the location of the probe shanks in the thalamus, we examined the tracks labeled by DiD in post-mortem brain sections. If part of a shank was located in the pulvinar, we analyzed activity along the length of the shank to define the dorsal and ventral nucleus borders. When channels were dorsal to the pulvinar, they typically were in the ventricle or in the hippocampus and seldomly had any units. The optrode contacts, which spanned 775 μm vertically, often extended past the ventral border of the pulvinar into POm. We defined this ventral border as the deepest contact which had a significantly visually responsive unit (See *Data Analysis* for statistical definition). For dLGN recordings, the ventral boundary was calculated in the same way.

Layer classification of cortical units

To assign units to cortical layers, we analyzed the CSD (Fig 2.1B) calculated from flashed, full-field stimuli (described above) with CSDPlotter in Matlab[66]. Channels which contained the earliest current sink were assigned to Layer 4. Channels dorsal to these channels were assigned to Layer 2/3. L5B typically exhibited another large sink that was delayed relative to the layer 4 sink and separated by weaker current (Layer 5A). Layer 6 was characterized by an

initial current source. Some recordings included white matter in the deepest channels, but no units were present on those channels to classify. Units typically had waveforms present on multiple channels, but were assigned to the channel and layer for which the waveform amplitude was largest. This CSD analysis was performed prior to the recording to confirm the depth of the probe as well as at the end of each recording to verify that no significant drift occurred due to probe movement or tissue relaxation.

Data analysis

For both thalamic and cortical units, we characterized the firing rates in response to visual stimuli with and without optogenetic stimulation. Locomotion significantly alters the gain of responses in the visual cortex and thalamus[67–69], so we excluded trials during which the mice ran at an average speed greater than 2 cm/s to reduce variability.

For cortical units, we restricted analysis to those units that were visually responsive. Units were classified as visually responsive if their firing rate for preferred trials (stimulus direction which evoked the largest firing rates during stationary, LED off trials) during the 1 ms stimulus period was significantly different than firing rates during blank trials (Wilcoxon rank-sum test with 0.05 significance level). 221 LM units from 7 mice met our cluster quality criteria. Of those, 155 units (70%) were visually responsive. For thalamic units, we calculated visual responsiveness to define nucleus boundaries, but included responsive and non-responsive pulvinar/dLGN units in our analysis.

To determine the effect of optogenetic stimulation on unit activity, we combined all visual stimulation trials and calculated the firing rates during the 1 ms stimulus presentation period for LED on and LED off trials separately. Significant modulation was determined with a Wilcoxon rank-sum test at 0.05 significance level with Benjamini-Hochberg correction for false

discovery rate. Firing rates for LED on and off trials were averaged and used to calculate a light modulation index (LMI) for each unit, defined as:

$$LMI = \frac{FR_{LED\ on} - FR_{LED\ off}}{FR_{LED\ on} + FR_{LED\ off}}$$

This metric ranges from -1 to 1, where negative values indicate suppression, and positive values indicate activation. For dLGN experiments, we fit a linear regression with no intercept to LED on firing rates as a function of LED off firing rates for units within 300-500 μm of the ventral dLGN border that were significantly suppressed. For both V1 and LM experiments, we fit a similar linear regression for all units regardless of firing rate modulation or layer. For LM experiments, we also compared the average firing rates with and without optogenetic inactivation for only preferred stimulus trials. For peri-stimulus time histograms, spikes were summed in 20 ms bins for each trial, and spike counts in each bin were averaged across trials for LED on and off trials separately.

We further sorted trials by visual stimulus and LED condition and calculated the average firing rates for each unique stimulus combination to generate orientation tuning curves. When spatial frequency and/or temporal frequency were varied, we calculated orientation tuning at the preferred sf and/or tf. Orientation selectivity index (OSI) was calculated as follows:

$$OSI = \frac{FR_{preferred} - FR_{orthogonal}}{FR_{preferred} + FR_{orthogonal}}$$

Where $FR_{preferred}$ is the average response to the preferred stimulus (maximum response), and $FR_{orthogonal}$ is the mean of the two directions orthogonal to the preferred stimulus. We compared the OSI values for LED on and off trials for the population of visually responsive LM units using the Wilcoxon sign-rank test at a 0.05 significance level with Benjamini-Hochberg correction for false discovery rate.

Lower signal to noise ratio and sparse firing of superficial units limited our ability to isolate many single units in layer 2/3. To evaluate whether thalamic inactivation had an effect on population firing that was not detected in single unit activity, we characterized the multi-unit activity in each cortical layer for one example experiment. Spike times from single unit clusters, regardless of quality metrics, were combined with spikes from clusters identified as MUA in phy for each channel. MUA on channels belonging to the same cortical layer were combined, and peri-stimulus time histograms were calculated with the same method used for single units (described above).

APPENDIX

Table 2.S1 Review of pulvinar inactivation studies with cortical activity measurements

Reference	Species	Brain State	Stimulus/task	Inactivation method	Results
Fang et al., 2020[36]	Mouse	Awake, passive viewing	Drifting gratings w/ varied sized, flashed white noise	Pharmacological (bupivacaine, muscimol) Optogenetic (ArchT in Pulvinar cells, Halo in Pulvinar terminals) DREADDi1	V1 L2/3 neurons increased firing rates, became less orientation and direction selective, and preferred larger sizes; V1 L4 unaffected
Eradath et al., 2021[37]	Macaque	Awake, passive viewing	Movie, no trial structure or controlled stimuli	Muscimol in dorsal lateral pulvinar	No change in cortical firing rates, decreased coherence between V4 and LIP
Zhou et al., 2016[19]	Macaque	Awake, behaving	Color change detection task	Muscimol in ventrolateral pulvinar	Sensory evoked: increased spontaneous rates, lower evoked responses Attention: reduced coherence between V4 and IT Behavioral: worse detection in attended RF
Purushothaman et al., 2012[38]	Galagos	Anesthetized	Drifting gratings	Muscimol in lateral pulvinar	Loss of visual responses in supragranular V1
Soares et al., 2004[39]	Cebus	Anesthetized	Moving oriented bar	Muscimol in lateral pulvinar	Mixed effects in V2 cells: 39% increased responses, 27% decreased responses; reduced orientation selectivity

ACKNOWLEDGEMENTS

Chapter 2 contains unpublished material coauthored with Professor Edward Callaway. The dissertation author was the primary author of this chapter.

REFERENCES

1. Jones, E. G. *The Thalamus*. (Springer US, 2012). at <https://books.google.com/books?id=myULCAAAQBAJ>

2. Molnár, Z. Development and Evolution of Thalamocortical Interactions. *European journal of morphology*. **38,** (2000).

3. Halley, A. C. & Krubitzer, L. Not all cortical expansions are the same: the coevolution of the neocortex and the dorsal thalamus in mammals. *Current Opinion in Neurobiology* **56,** 78–86 (2019).

4. Steriade, M., McCormick, D. A. & Sejnowski, T. J. Thalamocortical Oscillations in the Sleeping and Aroused Brain. *Science* **262,** 679–685 (1993).

5. Halassa, M. M. & Kastner, S. Thalamic functions in distributed cognitive control. *Nat Neurosci* **20,** 1669–1679 (2017).

6. Sommer, M. A. The role of the thalamus in motor control. *Current Opinion in Neurobiology* **13,** 663–670 (2003).

7. McCormick, D. A. & Bal, T. Sensory gating mechanisms of the thalamus. *Current Opinion in Neurobiology* **4,** 550–556 (1994).

8. Sherman, S. M. & Guillery, R. W. *Functional connections of cortical areas: a new view from the thalamus*. (MIT press, 2013).

9. Adams, M. M., Hof, P. R., Gattass, R., Webster, M. J. & Ungerleider, L. G. Visual cortical projections and chemoarchitecture of macaque monkey pulvinar. *J. Comp. Neurol.* **419,** 377–393 (2000).

10. Shipp, S. The functional logic of cortico–pulvinar connections. *Phil. Trans. R. Soc. Lond. B* **358,** 1605–1624 (2003).

11. Sherman, S. M. & Guillery, R. W. Distinct functions for direct and transthalamic corticocortical connections. *Journal of neurophysiology* **106,** 1068–1077 (2011).

12. Blot, A., Roth, M. M., Gasler, I., Javadzadeh, M., Imhof, F. & Hofer, S. B. Visual intracortical and transthalamic pathways carry distinct information to cortical areas. *Neuron* **109,** 1996-2008.e6 (2021).

13. Bender, D. B. & Youakim, M. Effect of Attentive Fixation in Macaque Thalamus and Cortex. *Journal of Neurophysiology* **85,** 219–234 (2001).

14. Saalmann, Y. B., Pinsk, M. A., Wang, L., Li, X. & Kastner, S. The Pulvinar Regulates Information Transmission Between Cortical Areas Based on Attention Demands. *Science* **337,** 753–756 (2012).

15. Petersen, S. E., Robinson, D. L. & Keys, W. Pulvinar nuclei of the behaving rhesus monkey: visual responses and their modulation. *Journal of Neurophysiology* **54,** 867–886 (1985).

16. Benevento, L. A. & Port, J. D. Single neurons with both form/color differential responses and saccade-related responses in the nonretinotopic pulvinar of the behaving macaque monkey. *Vis Neurosci* **12,** 523–544 (1995).

17. Grieve, K. L., Acuña, C. & Cudeiro, J. The primate pulvinar nuclei: vision and action. *Trends in Neurosciences* **23,** 35–39 (2000).

18. Robinson, D. L. & Petersen, S. E. The pulvinar and visual salience. *Trends in Neurosciences* **15,** 127–132 (1992).

19. Zhou, H., Schafer, R. J. & Desimone, R. Pulvinar-Cortex Interactions in Vision and Attention. *Neuron* **89,** 209–220 (2016).

20. Snow, J. C., Allen, H. A., Rafal, R. D. & Humphreys, G. W. Impaired attentional selection following lesions to human pulvinar: Evidence for homology between human and monkey. *Proc. Natl. Acad. Sci. U.S.A.* **106,** 4054–4059 (2009).

21. Rafal, R. D. & Posner, M. I. Deficits in human visual spatial attention following thalamic lesions. *Proc. Natl. Acad. Sci. U.S.A.* **84,** 7349–7353 (1987).

22. Danziger, S., Ward, R., Owen, V. & Rafal, R. The Effects of Unilateral Pulvinar Damage in Humans on Reflexive Orienting and Filtering of Irrelevant Information. *Behavioural Neurology* **13,** 95–104 (2002).

23. Arend, I., Rafal, R. & Ward, R. Spatial and temporal deficits are regionally dissociable in patients with pulvinar lesions. *Brain* **131,** 2140–2152 (2008).

24. Petersen, S. E., Robinson, D. L. & Morris, J. D. Contributions of the pulvinar to visual spatial attention. *Neuropsychologia* **25,** 97–105 (1987).

25. Wilke, M., Turchi, J., Smith, K., Mishkin, M. & Leopold, D. A. Pulvinar Inactivation Disrupts Selection of Movement Plans. *Journal of Neuroscience* **30,** 8650–8659 (2010).

26. Wilke, M., Kagan, I. & Andersen, R. A. Effects of Pulvinar Inactivation on Spatial Decision-making between Equal and Asymmetric Reward Options. *Journal of Cognitive Neuroscience* **25,** 1270–1283 (2013).

27. Chalupa, L. M., Coyle, R. S. & Lindsley, D. B. Effect of pulvinar lesions on visual pattern discrimination in monkeys. *Journal of Neurophysiology* **39,** 354–369 (1976).

28. Allen, A. E., Procyk, C. A., Howarth, M., Walmsley, L. & Brown, T. M. Visual input to the mouse lateral posterior and posterior thalamic nuclei: photoreceptive origins and retinotopic order. *J Physiol* **594,** 1911–1929 (2016).

29. Mathers, L. H. & Rapisardi, S. C. Visual and somatosensory receptive fields of neurons in the squirrel monkey pulvinar. *Brain Research* **64,** 65–83 (1973).

30. Rockland, K. S. Distinctive Spatial and Laminar Organization of Single Axons from Lateral Pulvinar in the Macaque. *Vision* **4,** 1 (2019).

31. Rockland, K. S., Andresen, J., Cowie, R. J. & Robinson, D. L. Single axon analysis of pulvinocortical connections to several visual areas in the Macaque. *J. Comp. Neurol.* **406,** 221–250 (1999).

32. Nakamura, H., Hioki, H., Furuta, T. & Kaneko, T. Different cortical projections from three subdivisions of the rat lateral posterior thalamic nucleus: a single-neuron tracing study with viral vectors. *Eur J Neurosci* **41,** 1294–1310 (2015).

33. Zhou, N., Masterson, S. P., Damron, J. K., Guido, W. & Bickford, M. E. The Mouse Pulvinar Nucleus Links the Lateral Extrastriate Cortex, Striatum, and Amygdala. *J. Neurosci.* **38,** 347–362 (2018).

34. Sherman, S. M. Thalamocortical interactions. *Current Opinion in Neurobiology* **22,** 575–579 (2012).

35. Beltramo, R. & Scanziani, M. A collicular visual cortex: Neocortical space for an ancient midbrain visual structure. *Science* **363,** 64–69 (2019).

36. Fang, Q., Chou, X., Peng, B., Zhong, W., Zhang, L. I. & Tao, H. W. A Differential Circuit via Retino-Colliculo-Pulvinar Pathway Enhances Feature Selectivity in Visual Cortex through Surround Suppression. *Neuron* **105,** 355-369.e6 (2020).

37. Eradath, M. K., Pinsk, M. A. & Kastner, S. A causal role for the pulvinar in coordinating task-independent cortico–cortical interactions. *Journal of Comparative Neurology* **529,** 3772–3784 (2021).

38. Purushothaman, G., Marion, R., Li, K. & Casagrande, V. A. Gating and control of primary visual cortex by pulvinar. *Nat Neurosci* **15,** 905–912 (2012).

39. Soares, J., Diogo, A., Fiorani, M., Souza, A. & Gattass, R. Effects of inactivation of the lateral pulvinar on response properties of second visual area cells in Cebus monkeys. *Clin Exp Pharmacol Physiol* **31,** 580–590 (2004).

40. Bennett, C., Gale, S. D., Garrett, M. E., Newton, M. L., Murphy, G. J. & Olsen, S. R. Higher-Order Thalamic Circuits Channel Parallel Streams of Visual Information in Mice. 19

41. Juavinett, A. L., Kim, E. J., Collins, H. C. & Callaway, E. M. A systematic topographical relationship between mouse lateral posterior thalamic neurons and their visual cortical projection targets. *J Comp Neurol* **528,** 99–111 (2020).

42. Sherman, S. M. Tonic and burst firing: Dual modes of thalamocortical relay. *Trends in Neurosciences* **24,** 122–126 (2001).

43. Mahn, M., Gibor, L., Patil, P., Cohen-Kashi Malina, K., Oring, S., Printz, Y., Levy, R., Lampl, I. & Yizhar, O. High-efficiency optogenetic silencing with soma-targeted anion-conducting channelrhodopsins. *Nat Commun* **9,** 4125 (2018).

44. Rosa, M. G. P. & Krubitzer, L. A. The evolution of visual cortex: where is V2? *Trends in Neurosciences* **22,** 242–248 (1999).

45. Whitmire, C. J., Liew, Y. J. & Stanley, G. B. Thalamic state influences timing precision in the thalamocortical circuit. *Journal of Neurophysiology* **125,** 1833–1850 (2021).

46. Reinagel, P., Godwin, D., Sherman, S. M. & Koch, C. Encoding of Visual Information by LGN Bursts. *Journal of Neurophysiology* **81,** 2558–2569 (1999).

47. Yizhar, O., Fenno, L. E., Davidson, T. J., Mogri, M. & Deisseroth, K. Optogenetics in Neural Systems. *Neuron* **71,** 9–34 (2011).

48. Essen, D. C. V. Corticocortical and thalamocortical information flow in the primate visual system. **149,** 173–185 (2005).

49. Zhou, N., Maire, P. S., Masterson, S. P. & Bickford, M. E. The mouse pulvinar nucleus: Organization of the tectorecipient zones. *Vis Neurosci* **34,** E011 (2017).

50. Kaas, J. H. & Baldwin, M. K. L. The Evolution of the Pulvinar Complex in Primates and Its Role in the Dorsal and Ventral Streams of Cortical Processing. *Vision* **4,** 3 (2019).

51. Robinson, D. L., Petersen, S. E. & Keys, W. Saccade-related and visual activities in the pulvinar nuclei of the behaving rhesus monkey. *Exp Brain Res* **62,** (1986).

52. Roth, M. M., Dahmen, J. C., Muir, D. R., Imhof, F., Martini, F. J. & Hofer, S. B. Thalamic nuclei convey diverse contextual information to layer 1 of visual cortex. *Nature Neuroscience* **19,** 148 (2015).

53. Gattass, R., P.B. Sousa, A. & Oswaldo-Cruz, E. Single unit response types in the pulvinar of the cebus monkey to multisensory stimulation. *Brain Research* **158,** 75–87 (1978).

54. Froesel, M., Cappe, C. & Ben Hamed, S. A multisensory perspective onto primate pulvinar functions. *Neuroscience & Biobehavioral Reviews* **125,** 231–243 (2021).

55. Schneider, L., Dominguez-Vargas, A.-U., Gibson, L., Kagan, I. & Wilke, M. Eye position signals in the dorsal pulvinar during fixation and goal-directed saccades. *Journal of Neurophysiology* **123,** 367–391 (2020).

56. Garrett, M. E., Nauhaus, I., Marshel, J. H. & Callaway, X. E. M. Topography and Areal Organization of Mouse Visual Cortex. **34,** 12587–12600 (2014).

57. Juavinett, A. L., Nauhaus, I., Garrett, M. E., Zhuang, J. & Callaway, E. M. Automated identification of mouse visual areas with intrinsic signal imaging. *Nat Protoc* **12,** 32–43 (2017).

58. Du, J., Blanche, T. J., Harrison, R. R., Lester, H. A. & Masmanidis, S. C. Multiplexed, High Density Electrophysiology with Nanofabricated Neural Probes. *PLoS ONE* **6,** e26204 (2011).

59. Yang, L., Lee, K., Villagracia, J. & Masmanidis, S. C. Open source silicon microprobes for high throughput neural recording. *J. Neural Eng.* **17,** 016036 (2020).

60. Siegle, J. H., López, A. C., Patel, Y. A., Abramov, K., Ohayon, S. & Voigts, J. Open Ephys: an open-source, plugin-based platform for multichannel electrophysiology. *J. Neural Eng.* **14,** 045003 (2017).

61. Pachitariu, M., Sridhar, S. & Stringer, C. *Solving the spike sorting problem with Kilosort*. (Neuroscience, 2023). doi:10.1101/2023.01.07.523036

62. Steinmetz, N. A., Aydin, C., Lebedeva, A., Okun, M., Pachitariu, M., Bauza, M., Beau, M., Bhagat, J., Böhm, C., Broux, M., Chen, S., Colonell, J., Gardner, R. J., Karsh, B., Kloosterman, F., Kostadinov, D., Mora-Lopez, C., O'Callaghan, J., Park, J., Putzeys, J., Sauerbrei, B., van Daal, R. J. J., Vollan, A. Z., Wang, S., Welkenhuysen, M., Ye, Z., Dudman, J. T., Dutta, B., Hantman, A. W., Harris, K. D., Lee, A. K., Moser, E. I., O'Keefe, J., Renart, A., Svoboda, K., Häusser, M., Haesler, S., Carandini, M. & Harris, T. D. Neuropixels 2.0: A miniaturized high-density probe for stable, long-term brain recordings. *Science* **372,** eabf4588 (2021).

63. Rossant, C., Kadir, S. N., Goodman, D. F. M., Schulman, J., Hunter, M. L. D., Saleem, A. B., Grosmark, A., Belluscio, M., Denfield, G. H., Ecker, A. S., Tolias, A. S., Solomon, S., Buzsáki, G., Carandini, M. & Harris, K. D. Spike sorting for large, dense electrode arrays. *Nat Neurosci* **19,** 634–641 (2016).

64. Hill, D. N., Mehta, S. B. & Kleinfeld, D. Quality Metrics to Accompany Spike Sorting of Extracellular Signals. *Journal of Neuroscience* **31,** 8699–8705 (2011).

65. Schmitzer-Torbert, N., Jackson, J., Henze, D., Harris, K. & Redish, A. D. Quantitative measures of cluster quality for use in extracellular recordings. *Neuroscience* **131,** 1–11 (2005).

66. Pettersen, K. H., Devor, A., Ulbert, I., Dale, A. M. & Einevoll, G. T. Current-source density estimation based on inversion of electrostatic forward solution: Effects of finite extent of neuronal activity and conductivity discontinuities. *Journal of Neuroscience Methods* **154,** 116–133 (2006).

67. Niell, C. M. & Stryker, M. P. Modulation of Visual Responses by Behavioral State in Mouse Visual Cortex. *Neuron* **65,** 472–479 (2010).

68. Erisken, S., Vaiceliunaite, A., Jurjut, O., Fiorini, M., Katzner, S., Busse, L., Reichardt, W. & Neuroscience, I. Effects of Locomotion Extend throughout the Mouse Early Visual System. *Current Biology* **24,** 2899–2907 (2014).

69. Aydın, Ç., Couto, J., Giugliano, M., Farrow, K. & Bonin, V. Locomotion modulates specific functional cell types in the mouse visual thalamus. *Nat Commun* **9,** 4882 (2018).